

Mario Rivera · Gregori A. Caignan

Recent developments in the ^{13}C NMR spectroscopic analysis of paramagnetic hemes and heme proteins

Received: 12 August 2003 / Revised: 7 October 2003 / Accepted: 10 October 2003 / Published online: 20 January 2004
© Springer-Verlag 2004

Abstract Despite the wealth of information that has been obtained from the study of paramagnetic hemes and heme proteins by ^1H NMR spectroscopy, there are certain limitations imposed by the nature of paramagnetically affected resonances that are difficult to overcome. Although it has long been recognized that ^{13}C NMR spectroscopy is likely to be a powerful complementary technique to overcome some of these limitations, the low sensitivity and low natural abundance of ^{13}C nuclei has resulted in a lag in the application of ^{13}C NMR spectroscopy to the study of paramagnetic hemes and heme proteins. The tremendous advances in methodology and instrumentation witnessed in the NMR field, coupled to the advent of recombinant DNA methods that have made possible the preparation and purification of significant quantities of proteins, and the biosynthesis of ^{13}C -labeled heme, have contributed to an increased interest in the study of paramagnetic heme active sites by ^{13}C NMR spectroscopy. As a consequence, ^{13}C NMR spectroscopy is emerging as a powerful tool to study heme electronic structure and structure–function relationships in heme-containing proteins. In this report we strive to summarize some of the recent developments in the analysis of paramagnetic hemes and heme-containing proteins by ^{13}C NMR spectroscopy.

Introduction

Heme-containing proteins and enzymes are vital components of most living organisms [1]. A common feature among heme proteins is the heme prosthetic group (protoheme IX) (Fig. 1), which upon interacting with the protein polypeptide, is capable of tuning its reactivity and performing a large variety of chemical functions. Hence, heme proteins participate in electron-transfer reactions (cyto-

chromes) [2], oxygen activation and insertion reactions (monooxygenases) [3], oxygen transport and storage (hemoglobin and myoglobin) [4], oxygen sensing in nitrogen-fixing bacteria (FixL) [5], heme metabolism (heme oxygenase) [6, 7], and regulatory functions based on nitric oxide (guanylyl cyclase, nitrophorins) [8, 9], to name a few. It is therefore important to elucidate how nature tunes the redox properties and reactivity of the ubiquitous heme within a protein so that the resultant activity is that of oxygen binding, oxygen activation, oxygen sensing, or electron transport at different redox potentials. In this context, the heme active site is a chromophore that is amenable to be studied by a variety of spectroscopic techniques, such as nuclear magnetic resonance (NMR), electron paramagnetic resonance (EPR), resonance Raman, electronic absorption, and magnetic circular dichroic (MCD) spectroscopies.

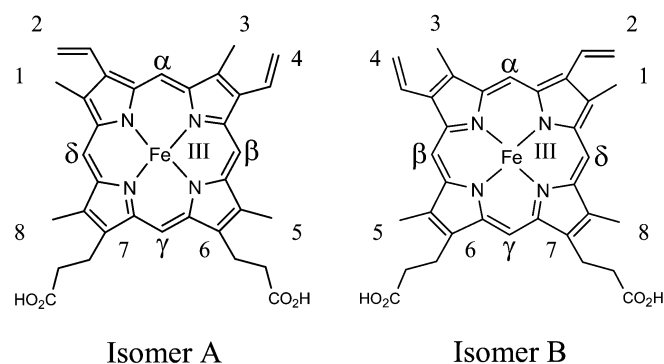
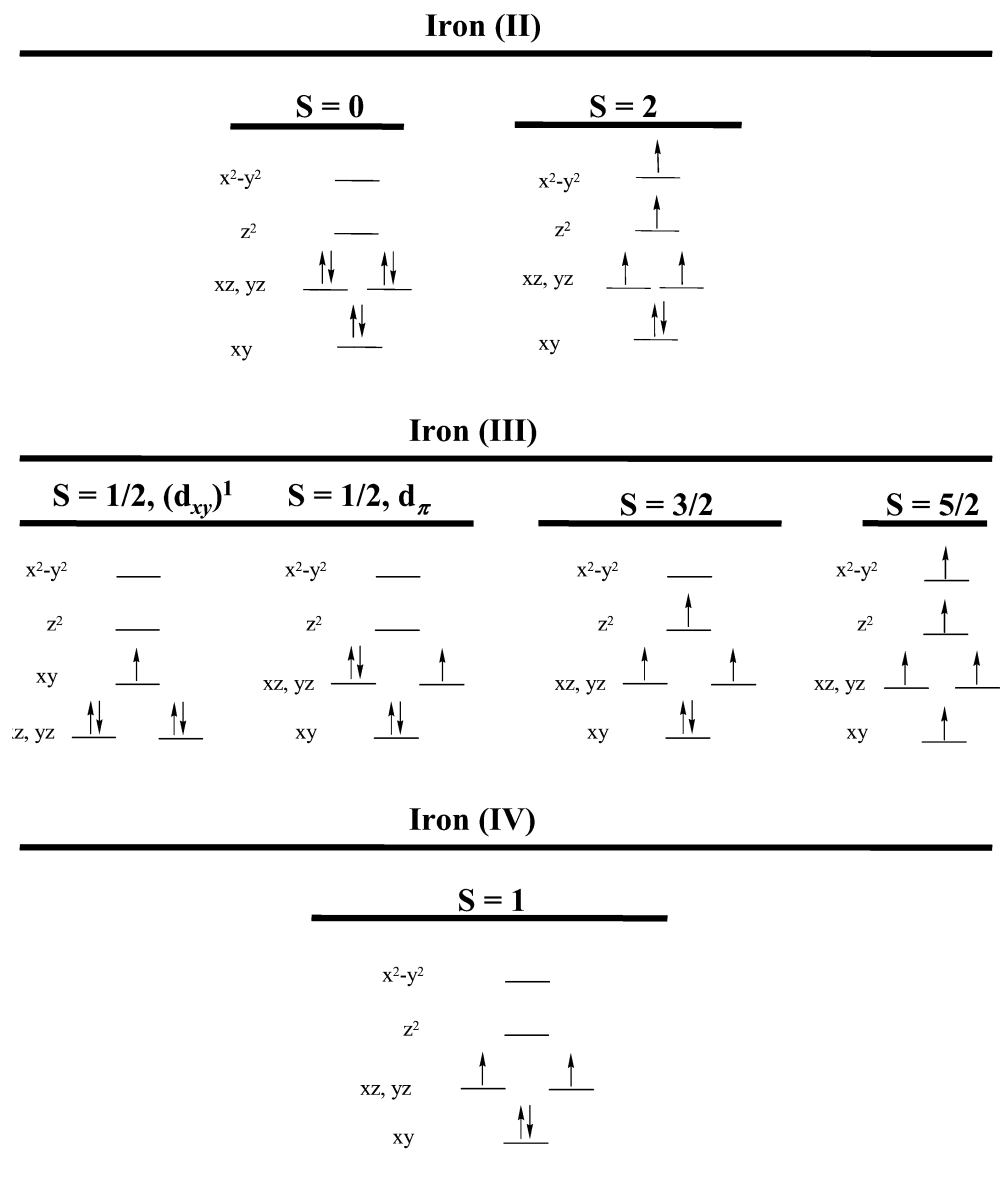


Fig. 1 Protoheme IX. The numbering scheme follows the Fisher nomenclature more commonly used in the magnetic resonance literature [15, 29]. By using this nomenclature the heme substituents are identified by their common names and a number indicating their position on the heme macrocycle (e.g., 1 methyl, 2 vinyl, 6 propionate). The substituents with more than one carbon are further characterized by the use of Greek letters to designate the number of bonds separating their carbons from the pyrrole ring (e.g., 2 vinyl- α , 6 propionate- β). In the asymmetric polypeptide fold, two heme isomeric forms (A and B) result from a 180° rotation of the heme about the α - γ meso axis

M. Rivera (✉) · G. A. Caignan
Contribution from the Department of Chemistry,
The University of Kansas, KS 66045–7582 Lawrence, USA
e-mail: mrivera@ku.edu

Fig. 2 Common spin states for the physiologically relevant oxidation states of iron

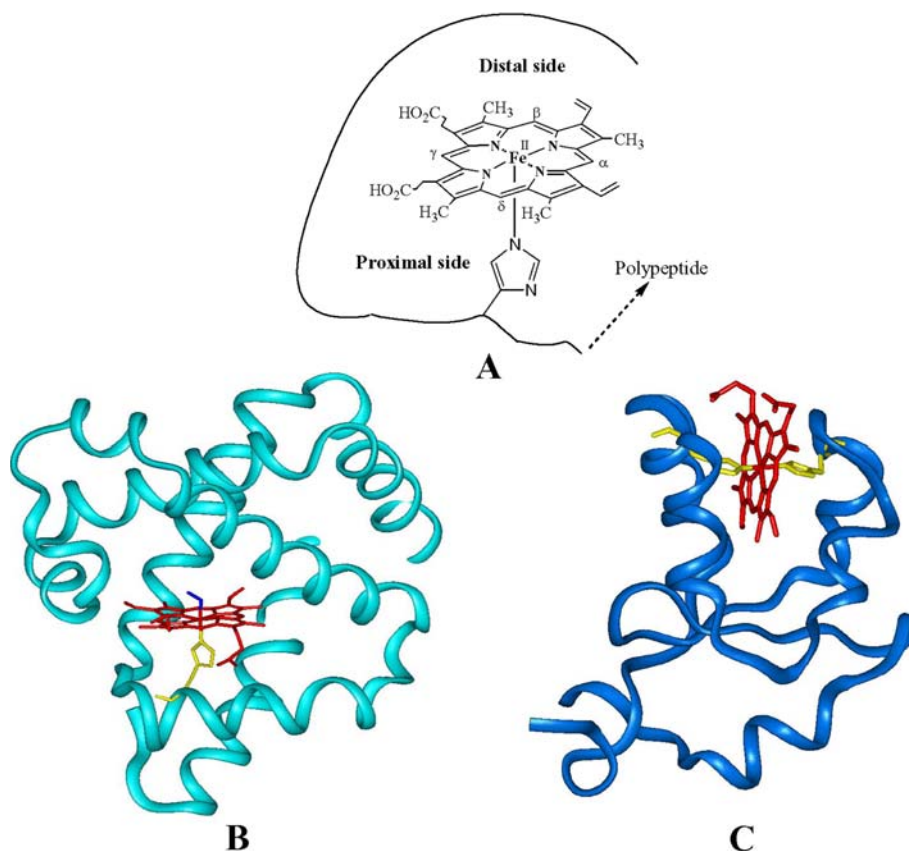


The oxidation state of the heme iron is an important modulator of the physical, chemical, and biochemical properties of heme proteins. For instance, myoglobin and hemoglobin form an oxyferrous complex, whereas the ferric oxidation state of these two heme proteins is non-functional. Electron-transfer proteins (cytochrome *b*₅, cytochrome *c*) have evolved to rapidly shuttle between the ferric and ferrous oxidation states, and oxygen-activating heme proteins (cytochrome P450, peroxidases) exhibit changes in the oxidation state of the heme iron (Fe^{II}, Fe^{III}, Fe^{IV}) as the reaction progresses through the catalytic cycle. It is therefore desirable to probe the heme active site in the different oxidation states.

The electronic structure of the heme changes with the oxidation and coordination state of the iron. Heme proteins can adopt different spin states as the relative energies of the metal orbitals are disrupted by endogenous (protein

donated) and exogenous ligands of varying field strengths (Fig. 2). For example, the heme iron in the deoxy form of hemoglobin and myoglobin is pentacoordinated; four equatorial positions are occupied by the pyrrole nitrogens in the heme, and one of the axial positions is occupied by a proximal histidine ligand, as shown schematically in Fig. 3A. The pentacoordinated Fe(II) in deoxymyoglobin adopts a high-spin, *S*=2 state. However, if an additional strong-field ligand, like O₂ or CO, coordinates opposite the proximal histidine (the distal side), the resulting hexacoordinated ferrous iron adopts a low-spin, *S*=0 configuration. This is illustrated by a view of the active site of oxymyoglobin in Fig. 3B. In a similar manner, ferric heme oxygenase, which is coordinated by an endogenous histidine and a weak-field water ligand on the distal side [10, 11] is found in the high-spin, *S*=5/2 state. Replacement of the water molecule by a strong-field ligand like cyanide

Fig. 3 **A** Schematic representation of the Fe(II) heme in deoxymyoglobin. **B** A view of the heme active site of oxymyoglobin, where the proximal histidine ligand is *yellow*, the heme is *red*, and the distal O₂ ligand is *blue* (PDB access code 1AJ6). A view of the active site of mitochondrial cytochrome *b*₅, where the heme (*red*) is coordinated by two axial histidine ligands shown in *yellow* (PDB access code is 1B5M)



produces a low-spin, $S=1/2$ state. By comparison, heme proteins that function in electron transfer are typically hexacoordinated in the ferric ($S=1/2$) as well as in the ferrous ($S=0$) oxidation states. The active site structure of the electron-transfer protein cytochrome *b*₅, in which the heme is coordinated by two axial histidine ligands, is shown in Fig. 3C. The coordination state of the heme iron often dictates the spin state, making the latter a useful tool to probe the ligation state of the metal center. More importantly, these coordination/spin state changes contribute to the mechanism of activity of all heme proteins, thus underscoring the importance of their investigation by spectroscopic means.

Heme complexes and heme proteins fall into the category of paramagnetic molecules, as all of the common iron electronic configurations, with the exception of Fe(II) low-spin, $S=0$, possess one or more unpaired electrons (Fig. 2). These unpaired electrons have a profound effect on the observed NMR chemical shifts as a consequence of the strong electron–nuclear hyperfine interaction. This interaction, which gives rise to the paramagnetic shift (δ_{para}) is composed of a scalar or contact contribution (δ_{con}) that arises from unpaired spin delocalization onto nuclei on the ligands, and a dipolar or through-space contribution, δ_{dip} (Eq. 1) [12]. The typically large chemical shifts observed for paramagnetically affected resonances (δ_{obs}) can be segmented into diamagnetic and paramagnetic contributions (Eq. 2).

$$\delta_{\text{para}} = \delta_{\text{con}} + \delta_{\text{dip}} \quad (1)$$

$$\delta_{\text{obs}} = \delta_{\text{dia}} + \delta_{\text{para}} \quad (2)$$

Thus, in order to isolate and analyze the paramagnetic (δ_{para}), also called isotropic (δ_{iso}) or hyperfine (δ_{hyp}) shifts, the corresponding chemical shifts of an isostructural diamagnetic molecule (δ_{dia}) should be subtracted from the observed shifts (Eq. 3) [13].

$$\delta_{\text{para}} = \delta_{\text{obs}} - \delta_{\text{dia}} \quad (3)$$

It is important to understand the nature of the contact and dipolar shift contributions in order to appreciate and interpret the information that can be obtained from paramagnetic shifts. The contact contribution to the paramagnetic shift is brought about by scalar coupling between electron spins and individual nuclei. When a single spin level with an isotropic g tensor is populated, and to the extent that Curie law is valid (usually approximately applicable for ferrihemes), the contact shift can be expressed by Eq. 4, where S is the total spin quantum number, g is the isotropic (average) g value, γ is the magnetogyric ratio of the nucleus in question, T is the absolute temperature, β is the Bohr magneton, k is the Boltzmann constant, and A is the hyperfine (scalar) coupling constant for coupling the spin of the electron to the spin of the nucleus of interest [14, 15, 16, 17, 18].

$$\delta_{\text{con}} = \frac{Ag\beta S(S+1)}{3\gamma_N\hbar kT} \quad (4)$$

Interpretation of the contact contribution to the ¹H paramagnetic shift in terms of metal ligand covalency is done

in the context of the McConnell equation [19] (Eq. 5), which relates the hyperfine coupling for each individual proton in an aromatic fragment (A^H) to the unpaired spin density at the carbon to which the proton is attached (ρ_C). Q_H is an empirical parameter (-63 MHz).

$$A^H = Q_H \rho_C \quad (5)$$

In the case of an aromatic carbon atom the hyperfine coupling constant A^C can be related to the spin density centered on its π orbital (ρ_C^π) and to the spin density centered on the π orbitals of the three atoms x_i bonded to it (ρ_{xi}^π) (Eq. 6) [20]. S^C accounts for spin polarization of the $1s$ orbital by unpaired spin density located on the p_z (π) orbital of the same carbon atom, Q_{Cxi} accounts for spin polarization of the $2s$ orbitals on neighboring carbons by unpaired π spin density on the observed carbon atom, and Q_{xiC} for spin polarization of the $2s$ electrons on the observed carbon atom by π spin density on the neighboring carbons [17, 21, 22, 23, 24].

$$A^C = (S^C + \sum_{i=1}^3 Q_{Cxi}^C) \rho_C^\pi + \sum_{i=1}^3 Q_{xiC}^C \rho_{xi}^\pi \quad (6)$$

For a methyl carbon atom bound to the pyrrole β carbon of heme, one obtains Eq. 7, where C' denotes the aromatic carbon to which the methyl group is bound ($Q_{C'C}^C \approx -39$ MHz) [18, 21, 25]. It is therefore clear that the δ_{con} contribution to the observed shift for a heme methyl carbon depends only on the unpaired electron density on the pyrrole β carbon to which the methyl carbon is bound. The relevance of Eq. 7 to the study of heme electronic structure by ^{13}C NMR spectroscopy will become evident later in this review.

$$A^C = Q_{C'C}^C \rho_{C'}^\pi \quad (7)$$

The dipolar contribution to the isotropic shift results from through-space interactions (dipole coupling) of the nuclear and electron magnetic moments. For heteronuclei (^{13}C) the δ_{dip} contribution to the isotropic shift consists of two terms, a metal centered (δ_{dip}^M) and a ligand centered (δ_{dip}^L) contribution. The term δ_{dip}^M results from coupling between the nucleus under observation and the unpaired spin density on the metal, and the term δ_{dip}^L results from coupling between the nucleus under observation and unpaired spin density on the p_z orbitals of the ligand. The δ_{dip}^L term is known to be small in low-spin ferrihemes [26], and in the case of heme substituents such as heme methyls, which do not participate directly in the delocalized π orbitals, δ_{dip}^L is negligible [25, 27]. A general expression for the predominant δ_{dip}^M contribution is given by Eq. 8:

$$\delta_{dip}^M = \frac{1}{12\pi \mu_0 N} \left\{ \left[\chi_{zz} - \frac{1}{2}(\chi_{xx} + \chi_{yy}) \right] \left(\frac{3\cos^2\theta - 1}{r^3} \right) + \frac{3}{2}(\chi_{xx} - \chi_{yy}) \left(\frac{\sin^2\theta \cos^2 2\Omega}{r^3} \right) \right\} \quad (8)$$

where r is the metal nucleus distance vector, N is Avogadro's number, χ_{ii} are the principal components of the magnetic susceptibility tensor, θ is the angle between the proton-metal vector and the z molecular axis, Ω is the angle

between the projection of the r vector on the xy plane and the x axis, and μ_0 is the vacuum permeability [15, 28, 29].

The linewidths of paramagnetically affected resonances can be very large as a consequence of the effect of the electron magnetic moment on nuclear relaxation. In the case of low-spin ferric hemes and relatively small heme proteins Curie relaxation [30, 31] can be ignored and the relaxation rate (R_{obs}) of a resonance in a paramagnetic system is expressed as the sum of paramagnetic (R_{para}) and diamagnetic (R_{dia}) terms (Eq. 9) [32].

$$R_{obs} = R_{para} + R_{dia} \quad (9)$$

The work of Solomon [33] and Bloembergen [34] pointed out that dipolar and contact interactions need to be considered to understand the effect of electron-nuclear interactions that lead to efficient nuclear relaxation. This topic has been reviewed exhaustively [35, 36]. Thus, the expressions for R_{1para} ($1/T_{1para}$) and R_{2para} ($1/T_{2para}$) describing the relaxation of a heme methyl carbon ($^{13}\text{CH}_3$) [32, 37] are given by Eqs. 10 and 11. The first term denotes nuclear relaxation through the electron-nuclear dipole-dipole interaction (dipolar relaxation) and the second term represents relaxation through hyperfine contact interactions between electrons and nuclei. Most constants have been previously defined; r_M and r_L represent the distance between the nucleus and the metal, and the $\text{C}_\beta\text{-}^{13}\text{CH}_3$ bond length, respectively, ρ is the unpaired electron density at the pyrrole β carbon (C_β) to which the $^{13}\text{CH}_3$ is bound, ω_C the ^{13}C nuclear resonance frequency, ω_S the electron resonance frequency, τ_c the correlation time for the dipolar interaction, and τ_e the correlation time for the contact exchange interaction. The dipolar exchange interaction τ_e comprises the rotational correlation time (τ_r), chemical exchange effects characterized by τ_{ex} , and electron relaxation time constants T_{1e} and T_{2e} (Eq. 12), whereas the contact interaction τ_e depends on T_{1e} and T_{2e} and τ_{ex} (Eq. 13).

$$\frac{1}{T_{1para}} = \frac{2}{15} [S(S+1)\gamma_C^2 g^2 \beta^2] \left[\frac{1}{r_M^6} + \frac{\rho^2}{r_L^6} \right] \left[\frac{\tau_c}{1 + (\omega_C - \omega_S)^2 \tau_c^2} + \frac{3\tau_c}{1 + \omega_C^2 \tau_c^2} + \frac{6\tau_c}{1 + (\omega_C + \omega_S)^2 \tau_c^2} \right] + \frac{2}{3} \left[\frac{S(S+1)A_{con}^2}{\hbar^2} \right] \left[\frac{\tau_e}{1 + (\omega_C - \omega_S)^2 \tau_e^2} \right] \quad (10)$$

$$\frac{1}{T_{2para}} = \frac{1}{15} [S(S+1)\gamma_C^2 g^2 \beta^2] \left[\frac{1}{r_M^6} + \frac{\rho^2}{r_L^6} \right] \left[4\tau_c + \frac{\tau_c}{1 + (\omega_C - \omega_S)^2 \tau_c^2} + \frac{3\tau_c}{1 + \omega_C^2 \tau_c^2} + \frac{6\tau_c}{1 + \omega_S^2 \tau_c^2} + \frac{6\tau_c}{1 + (\omega_C + \omega_S)^2 \tau_c^2} \right] + \frac{1}{3} \left[\frac{S(S+1)A_{con}^2}{3\hbar^2} \right] \left[\tau_e + \frac{\tau_e}{1 + (\omega_C - \omega_S)^2 \tau_e^2} \right] \quad (11)$$

$$\frac{1}{\tau_c} = \frac{1}{T_e} + \frac{1}{\tau_r} + \frac{1}{\tau_{ex}} \quad (12)$$

$$\frac{1}{\tau_e} = \frac{1}{T_e} + \frac{1}{\tau_{ex}} \quad (13)$$

In the case of large molecules such as heme proteins, expressions 10 and 11 can be simplified to Eqs. 14 and 15, respectively, where it can be seen that the rates of relaxation R_{1para} and R_{2para} for the heme methyl carbons are proportional to the unpaired electron density on the C_β carbon (ρ) to which the methyl carbon is bound [32]. These relationships (Eqs. 14 and 15) have been used to demonstrate that the paramagnetic terms do not contribute predominantly to the relaxation of the heme methyl carbon in ferric low-spin myoglobin. These findings are in stark contrast to the relaxation of heme peripheral protons, which is dominated by the paramagnetic contribution [37]. Thus, provided that the paramagnetic contributions are quantitatively estimated, it should be possible to interpret the relaxation behavior of carbon resonances in terms of internal molecular motion [37]. Despite its promise, this aspect of ^{13}C NMR spectroscopy applied to paramagnetic heme proteins has not yet been studied in detail or exploited to gain detailed understanding of the heme active site. Some of the reasons why ^{13}C NMR spectroscopy has not been widely used, a reality that seems to be rapidly changing, are discussed below.

$$\frac{1}{T_{1para}} = \frac{2}{5} [S(S+1)\gamma_C^2 g^2 \beta^2] \left[\frac{1}{r_M^6} + \frac{\rho^2}{r_L^6} \right] T_{1e} \quad (14)$$

$$\frac{1}{T_{2para}} = \frac{7}{15} [S(S+1)\gamma_C^2 g^2 \beta^2] \left[\frac{1}{r_M^6} + \frac{\rho^2}{r_L^6} \right] T_{1e} + \frac{1}{3} \left[\frac{S(S+1)A_{con}^2}{\hbar^2} \right] T_{1e} \quad (15)$$

^{13}C NMR spectroscopy in the analysis of heme proteins

The high sensitivity of the proton has led to an overwhelming emphasis on the utilization of ^1H NMR spectroscopy to study paramagnetic heme proteins [36, 38, 39, 40]. For these molecules ^1H NMR spectroscopy is capable of providing unique structural and electronic information for the heme active site and residues near the active site because of the large hyperfine shifts that result from unpaired electron density [12, 16, 29, 41, 42, 43]. Nevertheless, ^1H NMR spectroscopy of paramagnetic proteins has some fundamental limitations: (a) Asymmetric delocalization of unpaired electron density results in large isotropic shifts for some of the heme substituents but small to negligible isotropic shifts for others. This means that some of the resonances originating from the heme are resolved from the diamagnetic envelope of resonances and thus are relatively easy to observe, whereas other heme resonances are not resolved from the diamagnetic envelope and consequently their observation and assignment

are difficult. (b) Heme substituents in the reduced (usually diamagnetic) state lack isotropic shifts and are therefore difficult to examine by ^1H NMR spectroscopy. (c) Efficient spin-spin relaxation often makes through-bond proton-proton correlations in COSY and TOCSY experiments unobservable. The development of cross peak coherence in these experiments ($\pi J t = \pi/2$) requires that $t = 1/(2J)$. Hence, 70 ms and 35 ms, respectively, are required to develop cross peak coherences for vicinal ($J = 7$ Hz) and geminal ($J = 14$ Hz) ^1H - ^1H couplings. Since cross peak coherence must develop completely during the detection period, La Mar has pointed out that in the case of paramagnetic systems, where the condition $T_2^{-1} > ^3J_{\text{HH}}$ applies, the COSY cross peaks from signals with short T_2 values will be weak and sometimes undetectable [38, 44]. In fact, it has been proposed that the COSY cross peaks observed in paramagnetic systems originate from dipolar coupling and Curie spin-nuclear spin relaxation [44, 45]. By comparison, the larger heteronuclear coupling $^1J_{\text{CH}} \approx 140$ Hz requires only approximately 4 ms for the development of cross peak coherence, thus making heteronuclear correlation experiments immensely attractive when one is interested in studying paramagnetic heme centers by NMR spectroscopy. In diamagnetic molecules, connectivities are detected across portions of molecules without the use of small $^3J_{\text{HH}}$, using heteronuclear correlation experiments based on scalar ^{13}C - ^{13}C and ^{13}C - ^{15}N correlations. The relatively large value of the $^1J_{\text{CC}}$ (≈ 50 Hz) is much larger than typical $^3J_{\text{HH}}$; hence, similar experiments should be directly applicable to the observation and assignment of paramagnetically affected resonances.

Despite the potential utility of ^{13}C NMR spectroscopy in the study of paramagnetic proteins, until relatively recently, the inherent lower sensitivity of ^{13}C has largely limited the effective use of natural abundance ^{13}C NMR spectroscopy to observe resonances originating from the paramagnetic heme cofactor. In the 1970s and 1980s the most common application of ^{13}C NMR spectroscopy to the analysis of heme proteins involved the characterization of resonances originating from the distal carbon-monooxy (CO) ligand of heme proteins coordinated by a ^{13}C -enriched CO molecule [46, 47]. An early attempt to overcome the problems imposed by the low natural abundance of ^{13}C nuclei was to develop synthetic methods to introduce ^{13}C labels into the vinyl groups of the heme macrocycle [39, 48]. These pioneering experiments, which permitted the observation of ^{13}C resonances from heme vinyl groups in high-spin and low-spin myoglobin derivatives [39], demonstrated the practicality and importance of applying ^{13}C NMR spectroscopy to the analysis of paramagnetic heme proteins. More recently, the ^1H - ^{13}C COSY spectra of natural abundance ferricytochrome *c* [49] and that of sperm whale myoglobin [50], were utilized to assign the ^{13}C resonances originating from the heme methyl groups. Subsequently, the proton-detected heteronuclear multiple quantum coherence (HMQC) experiment [51] was utilized to identify several heme carbons and their corresponding proton resonances in the paramagnetic active site of cytochrome c_{550} [52], which culminated in the

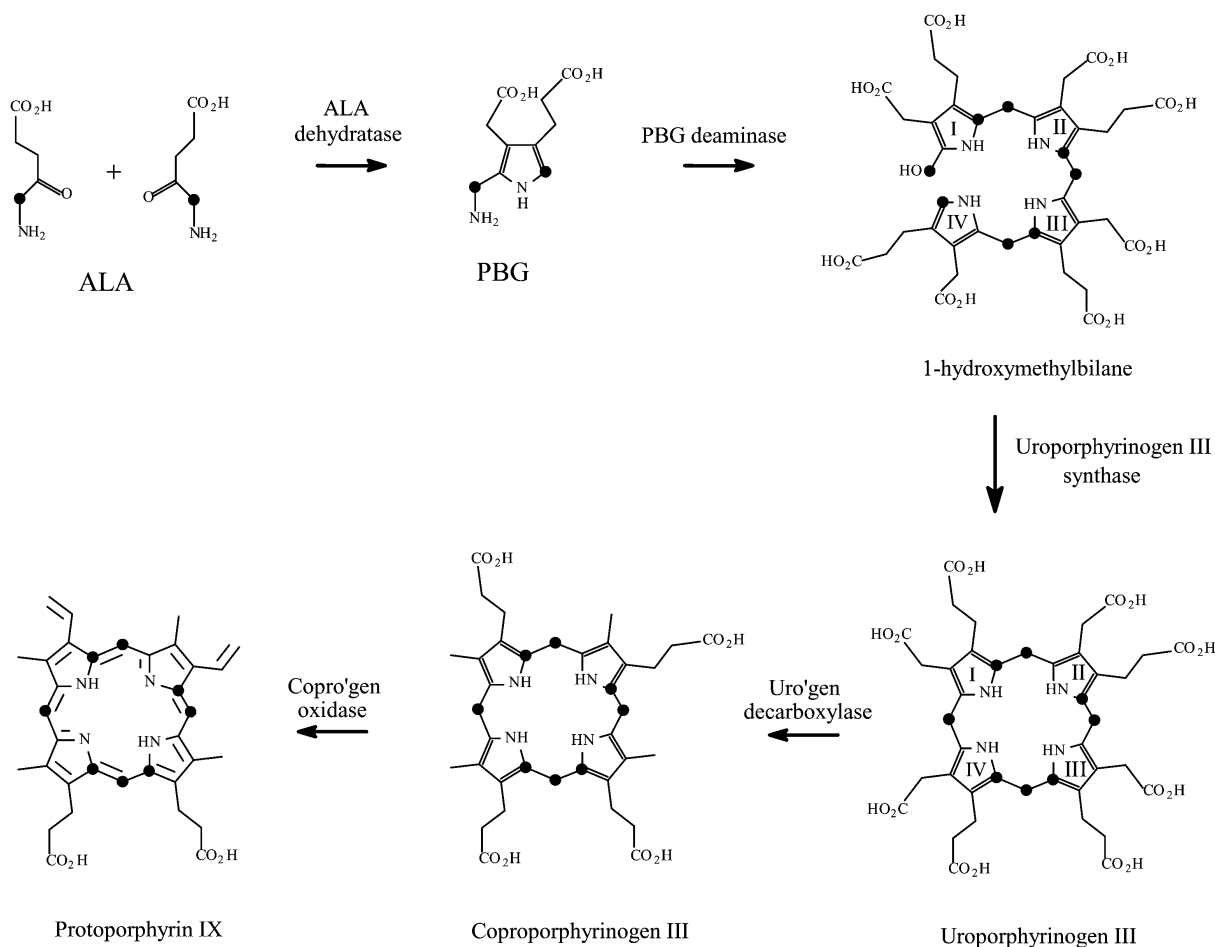


Fig. 4 Heme biosynthesis pathway; *highlighted atoms* are ^{13}C -labeled

assignment of most proton and carbon resonances for tuna ferricytochrome *c* [53]. This experiment has found widespread use in the identification of ^1H and ^{13}C resonances originating from protonated carbon atoms in paramagnetic heme centers [54, 55, 56]. However, resonances not resolved from the paramagnetic envelope are often difficult to assign, even with the aid of the HMQC experiment [57, 58]

Biosynthetic preparation of ^{13}C -labeled heme

A biosynthetic strategy that takes advantage of developments in recombinant DNA methodology and knowledge of the heme biosynthesis pathway has been developed to prepare isotopically enriched heme [59]. The first committed precursor in the biosynthetic pathway of heme is δ -aminolevulinic acid (ALA) [60, 61]. It can be seen from the biosynthetic pathway schematically shown in Fig. 4 that all atoms in the heme molecule are derived from ALA. Consequently, it should be possible to add isotopically enriched ALA to a growing bacterial culture in order to enhance heme biosynthesis and therefore obtain isotopically enriched heme [62, 63]. The problem with this

approach has been that when free protoporphyrin IX or free heme accumulate in the bacterial cell, intermediates in the biosynthetic pathway of heme such as coproporphyrinogen III and uroporphyrinogen III are excreted from the cell before they are converted into protoheme IX [62, 63], therefore causing isotopic dilution of the labeled precursor.

The problems caused by accumulation of free heme have been solved [59] by coupling the ability to control the biosynthetic pathway of heme with the bacterial overexpression of rat liver outer mitochondrial membrane cytochrome *b*₅ (OM *cyt b*₅), a heme binding protein [64]. Important in the success of this biosynthetic approach are the properties embedded in the expression system (pET 11a) [65]. The pET 11a plasmid maintains the OM *cyt b*₅ under control of strong bacteriophage T7 transcription and translation signals [65]. To initiate protein expression, the plasmid harboring the OM *cyt b*₅ gene is transferred into a host containing a chromosomal copy of the T7 RNA polymerase gene. The host, in this case the bacterial strain BL21(DE3), is a lysogen of the bacteriophage λDE3 , which contains the T7 RNA polymerase gene under control of the inducible lac UV5 promoter. T7 RNA polymerase is significantly more active than *E. coli* RNA polymerase. Consequently, once the transcription of the target gene (OM *cyt b*₅) has been induced the resources of the cell are used to aggressively transcribe the OM *cyt b*₅ gene located downstream from the T7 RNA polymerase promoter. When

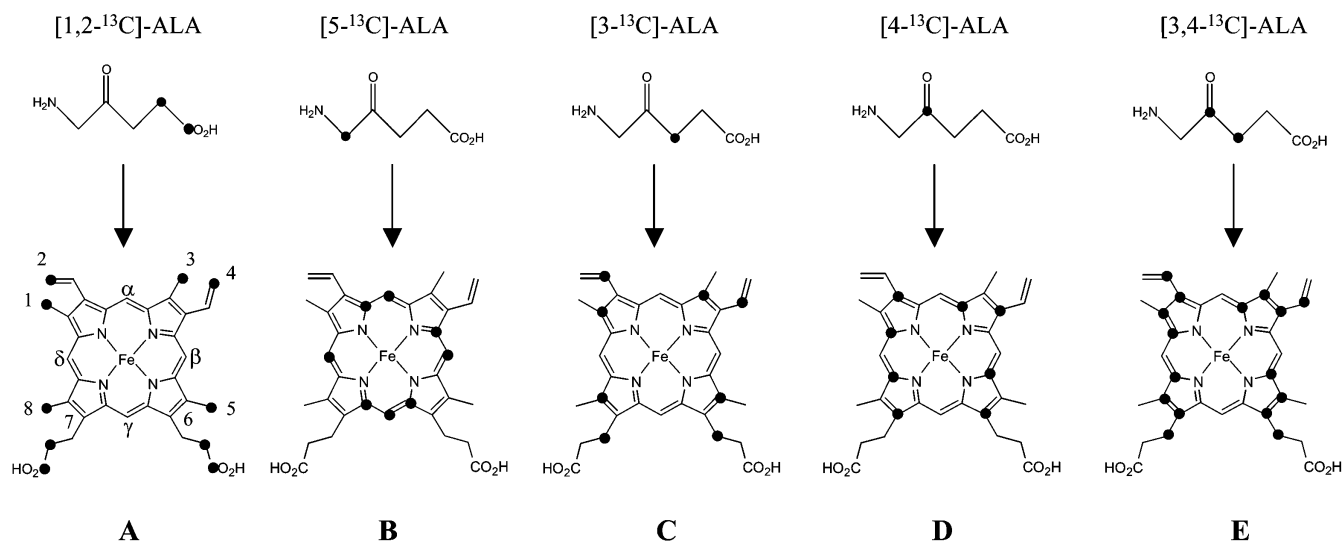


Fig. 5 ^{13}C -Labeling patterns obtained when protoporphyrin IX is biosynthesized from [1,2- ^{13}C]-ALA (A), [5- ^{13}C]-ALA (B), [3- ^{13}C]-ALA (C), [4- ^{13}C]-ALA (D) and [3,4- ^{13}C]-ALA (E). ● positions labeled with ^{13}C

this highly efficient expression of OM cyt b_5 is coupled to the enhanced biosynthesis of heme, which is brought about by the addition of exogenous labeled ALA, the following advantages are obtained:

- E. coli* cells are grown in the absence of labeled ALA until a critical mass of bacteria is obtained [64].
- When the overexpression of OM cyt b_5 is induced with simultaneous addition of a suitably labeled ALA, labeled heme is rapidly produced and subsequently sequestered by apo-OM cyt b_5 . The rates of heme release from OM cyt b_5 are much slower than those for heme release from microsomal cytochromes b_5 and other heme proteins [66, 67, 68]. Consequently, the incorporation of newly synthesized heme into apo-OM cyt b_5 avoids the accumulation of free heme, thereby preventing the undesirable isotopic scrambling.
- Purification of the labeled heme is straightforward since it is co-purified with OM cyt b_5 in two chromatographic steps.
- Because the heme in OM cyt b_5 is not covalently attached to the polypeptide, the macrocycle can be easily extracted from the protein and used to reconstitute other heme proteins with removable hemes [69, 70].

The fact that labeled heme is synthesized in *E. coli* according to the pathway summarized in Fig. 4 means that a judicious choice of labeled precursor (ALA) must be made in order to facilitate the assignment of the heme resonances of interest. For example, when [1,2- ^{13}C]- δ -amino-levulinic acid ([1,2- ^{13}C]-ALA) is used as a heme precursor, heme labeled at the four methyl, two vinyl β , two heme propionate β , and two carbonyl carbons is obtained [59, 71] (Fig. 5A). In a similar manner, heme labeled at all four *meso* and selected pyrrole α carbons can be obtained by utilizing [5- ^{13}C]-ALA as a heme precursor (Fig. 5B).

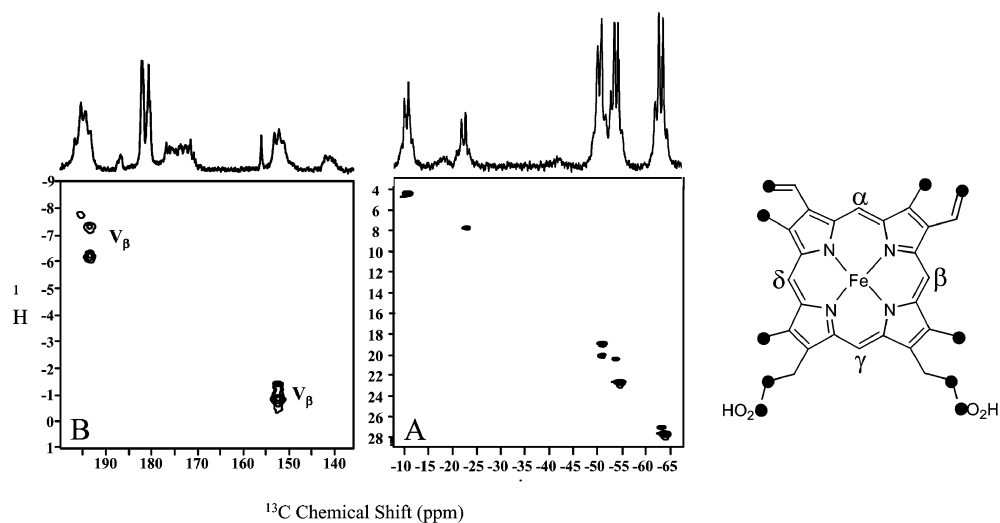
^{13}C -labeling schemes that have been utilized in the study of heme proteins, together with their corresponding isotopically marked ALA precursors, are summarized in Fig. 5 [59, 69, 70, 71, 72, 73, 74]. The usefulness of the biosynthetic methods described above depends on the availability of labeled ALA precursors, such as those shown in Fig. 5, in order to facilitate the preparation of labeled hemes. Although a few singly labeled ALAs are commercially available, several of the doubly and singly labeled ALAs of Fig. 5 are not. This problem has been somewhat circumvented by the development and description of simple synthetic routes for the preparation of the ^{13}C -labeled ALAs shown in Fig. 5. These synthetic methods utilize relatively inexpensive and readily available ^{13}C -labeled starting materials [75, 76].

In a related approach, the heme propionate carbonyl carbons of heme A in cytochrome *c* oxidase from *Paracoccus denitrificans* were labeled with ^{13}C for subsequent FTIR difference spectroscopic studies [77]. This was accomplished by deleting the *hemA* gene of the *P. denitrificans* strain PD1222 that codes for 5-aminolevulinic acid synthase, which is the enzyme that catalyzes the condensation of glycine and succinyl-coenzyme A to form δ -amino-levulinic acid. Since *P. denitrificans* possesses only one gene locus for ALA synthase (*HemA*), deletion of this gene results in heme auxotrophy [78]. Supplementation of the growth medium with ALA restored normal growth and when [1- ^{13}C]-ALA was added the carbonyl carbons of heme A in cytochrome *c* oxidase were labeled with high efficiency [77].

Resonance assignment strategies that capitalize on the availability of ^{13}C -labeled heme

The assignments of resonances originating from paramagnetic heme active sites are typically carried out with the aid of one- and two-dimensional ^1H NMR spectroscopic experiments [29]. Hence, assignments are carried out with experiments that are based on ^1H - ^1H scalar correlations

Fig. 6A,B Low (A) and high (B) frequency (^{13}C) portions of the HMQC spectrum of cyanide-inhibited heme oxygenase from *Pseudomonas aeruginosa* heme oxygenase (*pa*-HO-CN) reconstituted with heme derived from [1,2- ^{13}C]-ALA showing both contour plot and 1-D ^{13}C spectrum. Reprinted from reference [69]



(COSY), heteronuclear scalar correlations (HMQC and HSQC), and homonuclear dipolar correlations, in much the same way in which assignments are obtained for diamagnetic molecules. The most important distinction is that rapid relaxation induced by the unpaired electron(s) has the effect of lowering the intensities of cross peaks and compromising the effectiveness of pulse sequences that incorporate several delays [29]. For instance, the deleterious impact that short T_2 values have on the detectability of COSY cross peaks has been discussed above. Despite these difficulties, through careful tailoring of parameters to account for the fast relaxation imparted to the signals by the unpaired electron(s), ^1H NMR spectroscopy has been successfully used to provide a wealth of information about the physical, chemical, and dynamic properties of heme active sites in heme proteins and heme-containing enzymes [12, 16, 29, 41, 42, 43]. However, the assignment of heme resonances not resolved from the envelope of diamagnetic resonances in moderately large heme proteins, or in heme proteins that exist as a mixture of two heme orientational isomers, or in more complex mixtures involving heme isomerism and more than one heme seating, can still be problematic. As will be discussed below, these problems can be overcome, or at least attenuated by employing heme proteins reconstituted with ^{13}C -labeled heme to carry out the assignments.

^{13}C NMR spectroscopy has been recently utilized to obtain the assignments of resonances originating from heme substituent groups in the paramagnetic, cyanide-inhibited, ferric state of the enzyme heme oxygenase from *Pseudomonas aeruginosa* [69]. The assignments were carried out with the aid of labeled heme obtained from [1,2- ^{13}C]-ALA and [5- ^{13}C]-ALA (Figs. 5A and B, respectively). The sample reconstituted with heme labeled as in Fig. 5A allowed the efficient identification of all methyl carbon resonances, which are located between -10 and -65 ppm (see Fig. 6). These resonances can be readily attributed to heme methyl groups because they display the typical $^1J_{\text{CH}} \approx 140$ Hz quartets. Note that labeling only the heme active site and not the polypeptide permits the ready

identification of methyl ^1H signals in the HMQC spectrum, including those that would normally be obscured by the diamagnetic signals, approximately 4 and 8 ppm in the ^1H dimension of the spectrum of Fig. 6A. The eight cross peaks originating from heme methyl resonances, instead of the expected four from each of the four methyl groups in heme, stem from the coexistence of two heme orientational isomers (see Fig. 1). The labeling scheme of Fig. 5A also permits the straightforward identification of resonances originating from heme vinyl β and heme propionate β groups. These are readily discernable, because vinyl β carbons display a $^1J_{\text{CH}}$ triplet (Fig. 6B), whereas propionate β carbons, which are located next to the ^{13}C -labeled carbonyls, exhibit triplets ($^1J_{\text{CH}} \approx 140$ Hz) of doublets ($^1J_{\text{CC}} \approx 55$ Hz).

The assignments of heme resonances are typically obtained with the aid of NOESY experiments [12, 29]. The labeling pattern obtained from [5- ^{13}C]-ALA provides a unique entry point to interpret the NOESY map. This entry point is provided by the fact that one of the *meso* carbons (all four are labeled) is unique in that it is not bonded to a ^{13}C -labeled pyrrole α carbon, and therefore produces a $^1J_{\text{CH}}$ doublet. By comparison, the resonances arising from *meso* carbons adjacent to ^{13}C -labeled pyrrole α carbons consist of AMX quartets, that is, a $^1J_{\text{CH}}$ doublet further split by a $^1J_{\text{CC}}$ coupling. This situation is clearly seen in the spectrum of OM cytochrome b_5 reconstituted with heme labeled as in Fig. 5B. This protein exists in solution as an equimolar mixture of two heme orientational isomers and the corresponding one-dimensional ^{13}C NMR spectrum is shown in Fig. 7. It can be seen that the α -*meso* carbons from isomers A and B (ca. 55 ppm) exhibit clearly defined AMX quartets in the one-dimensional ^{13}C NMR spectrum. A similar situation is observed for *meso* carbon β in isomer A (≈ 23 ppm) and *meso* carbon γ (≈ 28 ppm) in isomer B. By comparison, the peak originating from *meso* carbon δ in isomer A (16 ppm) is clearly a $^1J_{\text{CH}}$ doublet, hence, providing a unique entry point that permits the dipolar correlations and therefore assignment of heme resonances originating from isomer A [72]. It is interesting to

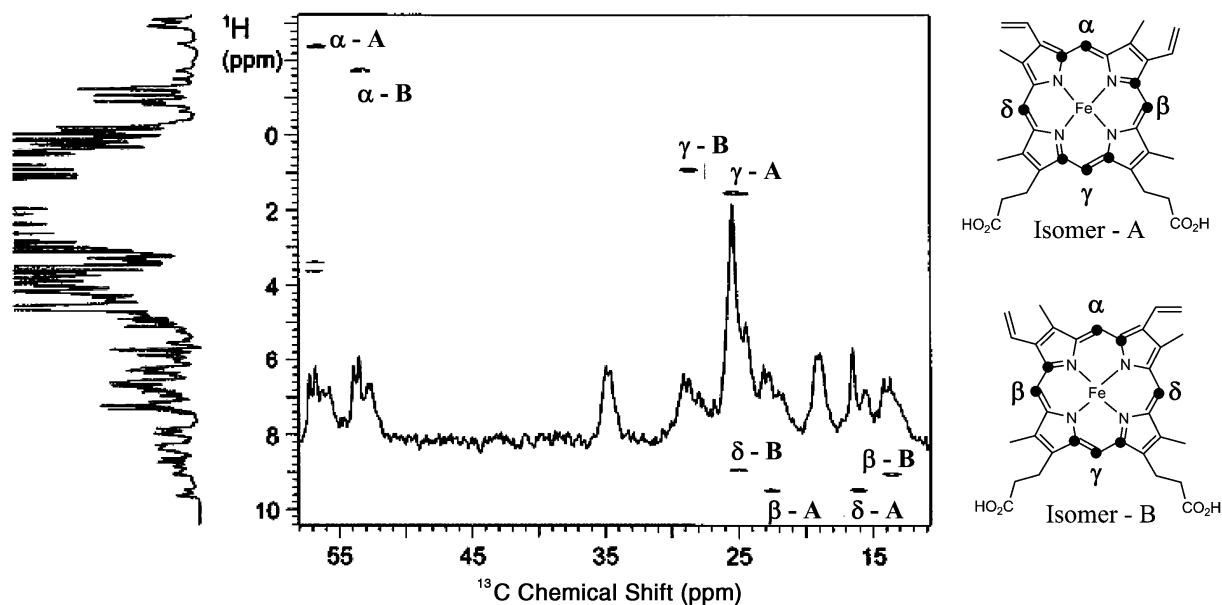


Fig. 7 A portion of the HMQC spectrum obtained with a sample of OM cytochrome *b*₅ containing heme biosynthesized from [5-¹³C]-ALA. The labeled carbon atoms in both heme isomers are highlighted by ●. The 1-D ¹³C NMR spectrum, which was acquired without ¹H decoupling, is included to illustrate the asymmetric linewidths within each multiplet. Adapted from reference [72]

point out that within each AMX quartet the doublet at higher frequency is sharper than the doublet at lower frequency. This is believed to originate from cross correlation between Curie relaxation and dipole–dipole relaxation [72], which resembles the cross correlation between dipole–dipole relaxation and chemical shift anisotropy relaxation that has been utilized to increase the accessible size of molecules that can be studied by solution-state NMR [79].

In cases where unambiguous assignments cannot be obtained with the strategy described above, it is possible to label the heme using [3-¹³C]-ALA as a precursor, which results in the isotopic labeling of heme vinyl α and heme propionate α carbons (Fig. 5C). Thus, the three labeling schemes, Figs. 5A–C, permit the relatively straightforward identification of the ¹H and ¹³C resonances originating from all protonated groups in the heme. This has the effect of largely facilitating the identification of heme resonances located under the intense envelope of diamagnetic resonances, thus making the interpretation of dipolar correlations significantly less ambiguous.

In diamagnetic molecules the assignment of quaternary carbons is ordinarily obtained from the heteronuclear multiple bond correlation (HMBC) experiment [51]. In paramagnetic molecules, however, the relatively long delays of the HMBC experiment (${}^2J_{CH}$) are at odds with fast relaxation ($T_2^{-1} > {}^2J_{CH}$), and this is typically manifested in the absence of long-range correlations. The relatively larger values of ${}^1J_{CC}$ make double quantum coherence experiments (¹³C–¹³C) attractive for the assignment of quaternary carbons in paramagnetic heme centers, provided

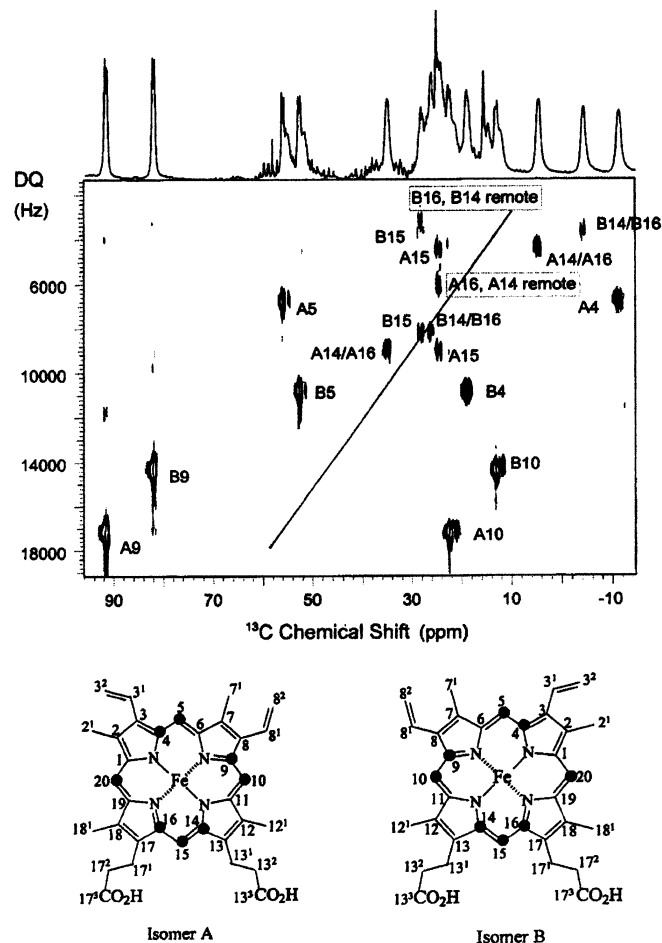
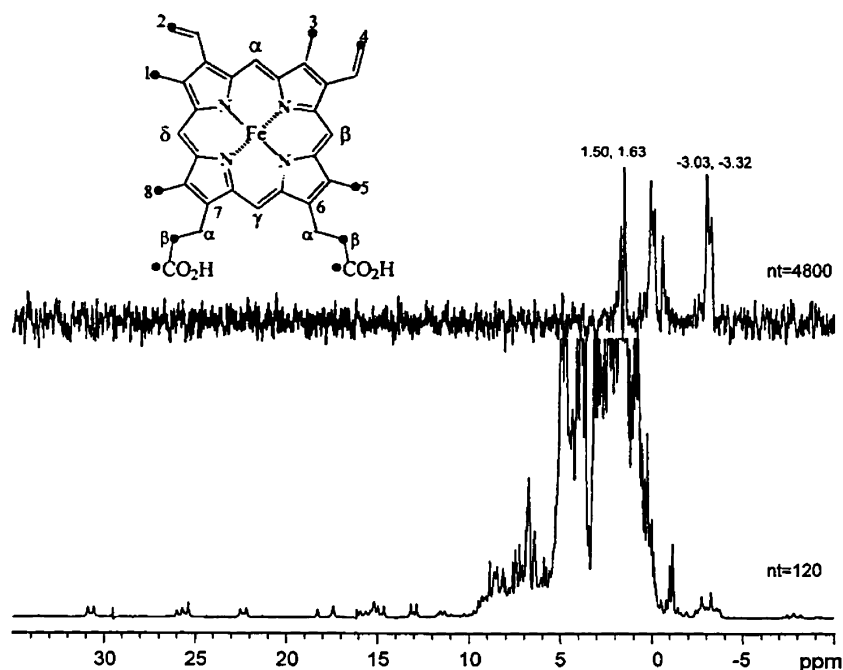


Fig. 8 INADEQUATE spectrum obtained with a sample of OM cytochrome *b*₅ containing heme derived from [5-¹³C]-ALA. The labeled carbons in both heme isomers are highlighted by ●. The IUPAC nomenclature was used for numbering and a preceding A or B was added to distinguish the heme isomers which result from a 180° rotation around the 5–15 *meso* carbon axis. Adapted from reference [72]

Fig. 9 Top DRIED (^1H - ^{13}C - ^{13}C) spectrum obtained with a sample of OM cytochrome b_5 -containing heme derived from [1,2- ^{13}C]-ALA. Bottom traditional one pulse experiment. Adapted from reference [81]



that heme labeled at adjacent carbon atoms is available. Cytochrome b_5 reconstituted with heme labeled as in Figs. 5B and E was used to test the applicability of the ^{13}C - ^{13}C double quantum coherence (INADEQUATE) [80] experiment for the detection and assignment of quaternary carbons in paramagnetic heme proteins [72]. The INADEQUATE spectrum in Fig. 8 makes it evident that the assignment of several pyrrole C_α carbons can be obtained from previously assigned *meso* carbons (see above) via ^{13}C - ^{13}C double quantum correlations. Moreover, a judicious choice of labeling scheme can render a wealth of information regarding core porphyrin carbons with a minimum number of experiments. For instance, all pyrrole C_β carbons and several pyrrole C_α carbons have been assigned with the aid of ^{13}C - ^{13}C double quantum coherence correlations departing from the assignments corresponding to the highlighted protonated carbons in each pyrrole ring of the macrocycle labeled as in Fig. 5E [72].

In keeping with the advantages furnished by the relatively large values of $^1J_{\text{CH}}$ and $^1J_{\text{CC}}$ a new NMR experiment was devised which selectively detects ^1H in $^1\text{H}_n$ - ^{13}C - ^{13}C fragments [81]; these fragments were introduced biosynthetically into heme by using [1,2- ^{13}C]-ALA as a heme precursor. The new experiment, double-resonance isotope-edited (DRIED), combines the well-known INEPT sequence [82] to transfer ^1H magnetization to ^{13}C nuclei, followed by INADEQUATE to generate ^{13}C - ^{13}C double quantum coherence between directly bound ^{13}C atoms [80], and finally reverse INEPT to detect the results through the sensitive ^1H nuclei. By combining the INEPT and INADEQUATE building blocks the DRIED experiment takes advantage of the relatively short interpulse delays permissible by $^1J_{\text{CH}}$ and $^1J_{\text{CC}}$, thus avoiding the long interpulse delays that in HMBIC compromise the detection of rapidly relaxing nuclei. The DRIED experiment allowed

exclusive observation of the diastereotopic heme propionate β protons in cytochrome b_5 , Fig. 9, where the ^1H - ^{13}C - ^{13}C -edited spectrum (top trace) is compared to the traditional one-pulse experiment (bottom trace).

^{13}C NMR chemical shifts of quaternary carbons and heme electronic structure

The observation and assignment of core porphyrin carbons is more challenging than that of protonated heme carbons because of their closer proximity to the heme iron, which makes these carbons more strongly affected by the unpaired electron. However, as will be discussed below, there is a straightforward correlation between the chemical shifts of these core carbons and the coordination state and electronic structure of the heme, which warrants the effort needed to observe and assign these resonances. Recent studies conducted with low-spin ferriheme complexes have contributed to solidifying the idea that chemical shifts originating from porphyrin core carbons, C_α , C_β , and C_{meso} (C_m) greatly facilitate the assessment of electronic structure [83, 84, 85, 86, 87]. Furthermore, calculations utilizing density functional theory methods have recently been used to successfully predict the chemical shift of core carbon resonances from hemes exhibiting different oxidation and spin states [88]. As an example of the usefulness of observing core carbon resonances it is illustrative to consider the two electronic configurations attained by low-spin ferrihemes: the more common $(d_{xy})^2(d_{xz}, d_{yz})^3$ electronic configuration is typically abbreviated d_π because the unpaired electron resides in one of the d_π orbitals, and the less common $(d_{xz}, d_{yz})^4(d_{xy})^1$ configuration is commonly abbreviated $(d_{xy})^1$ because the unpaired electron resides in the d_{xy} orbital (see Fig. 2) [15,

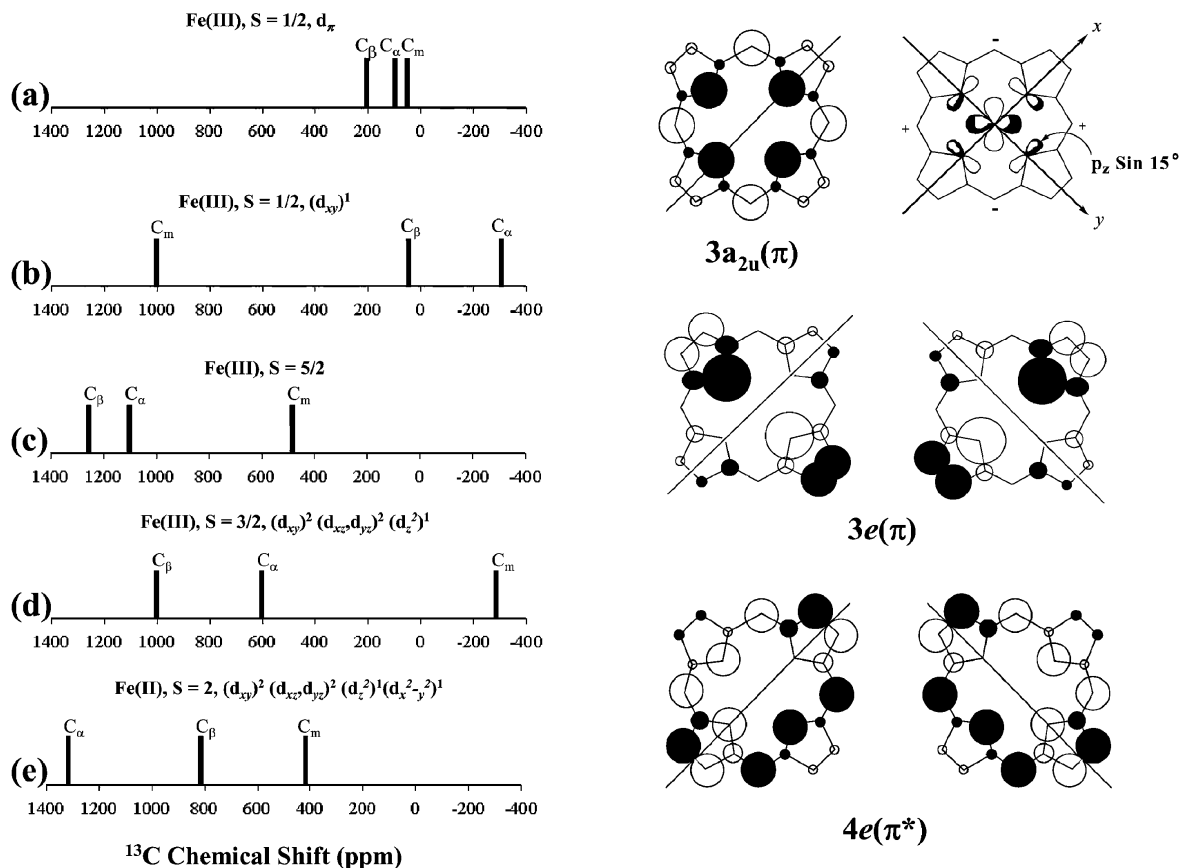


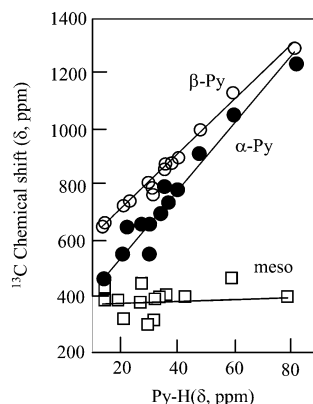
Fig. 10a–e Chemical shifts characteristic of core C_α , C_β , and C_m carbons. **a** Fe^{III} -porphyrinates with the $S=1/2$, d_π electron configuration, **b** Fe^{III} -porphyrinates with the $S=1/2$, $(d_{xy})^1$ electron configuration, **c** Fe^{III} porphyrinates with the $S=5/2$ electron configuration, **d** Fe^{III} -porphyrinates with the $S=3/2$, $(d_{xy})^2(d_{xz},d_{yz})^2(d_z^2)^1$ electron configuration, and **e** Fe^{II} -porphyrinates with the $S=2$ electron configuration. The C_α and C_β resonances of deoxymyoglobin ($S=2$) have been reported to occur near 850 ppm [139]; however, density functional theory calculations predict the C_α resonance between 1,040 and 1,400 ppm. *Right* schematic representation (adapted from reference [15]) of the $3a_{2u}(\pi)$, $3e(\pi)$, and $4e(\pi^*)$ porphyrin orbitals. The relative size of the *circles* at each atom are proportional to the calculated electron density. The possible interactions between the d_{xy} orbital and the porphyrin nitrogens of a ruffled porphyrin which allow spin delocalization into the $3a_{2u}(\pi)$ orbital are shown schematically next to this orbital

89, 90]. Spin delocalization in ferrihemes with the common $S=1/2$, d_π electronic structure is mainly into the porphyrin $3e(\pi)$ orbital shown schematically in Fig. 10. It can be seen from the relative sizes of the circles in this schematic representation that the C_β carbons possess relatively large electron density, the C_α carbons possess relatively small electron density, and the C_m carbons have zero electron density. Thus, the corresponding shifts are located at about 200 ppm for C_β carbons, approximately 100 ppm for C_α carbons, and about 70 ppm for C_m carbons (Fig. 10a) [23, 72]. By comparison spin delocalization in ferrihemes with the less common $S=1/2$, $(d_{xy})^1$ electronic configuration is mainly into the $3a_{2u}(\pi)$ orbital [15], which exhibits large electron density at the C_m carbons and small electron density at the C_α and C_β carbons (Fig. 10). Con-

sequently, ferrihemes possessing the $(d_{xy})^1$ electron configuration display large downfield C_m shifts ($\approx 1,000$ ppm), relatively large upfield C_α shifts (≈ 300 ppm), and small C_β shifts (≈ 20 – 70 ppm) (Fig. 10b). Since the $3a_{2u}(\pi)$ orbital has a very small spin density at the C_α position, the relatively large upfield C_α shifts are a consequence of spin polarization from the C_m carbons [84]. It should be pointed out that Fe^{III} -porphyrinates with the $S=1/2$, $(d_{xy})^1$ electron configuration are significantly ruffled [91] so that the nodal planes of the p_z orbitals are no longer in the xy plane; hence, the projections of these p_z orbitals have the proper symmetry to interact with the d_{xy} orbital, as has been shown schematically in Fig. 10 [91].

In the case of ferric porphyrinates exhibiting the high-spin, $S=5/2$ state, half occupation of the $d_{x^2-y^2}$ orbital results in large spin delocalization to all core carbons via σ bonds [41, 88, 92, 93], which results in very large downfield shifted chemical shifts for C_α ($\approx 1,100$ ppm) and C_β ($\approx 1,300$ ppm) carbons (Fig. 10c). The *meso* carbons shifts are still downfield and large (≈ 450 ppm) [83, 87]; however, these shifts are related to π spin delocalization from one of the d_π orbitals into the $4e(\pi^*)$ orbital, which has large electron density at the *meso* positions (Fig. 10) [15, 41, 88, 94]. The heme active site in proteins exhibiting the ferric high-spin, $S=5/2$ state is typically hexacoordinated, with a proximal histidine and a distal water ligand. Examples of this coordination state are met-hemoglobin and met-myoglobin from horse heart or sperm whale [4]. Alternatively, the ferric high-spin, $S=5/2$ state in heme proteins can also be pentacoordinated, where only a protein

Fig. 11 Correlation of the ^{13}C chemical shifts of C_α , C_β , and C_m carbons against the ^1H chemical shifts of the pyrrole hydrogens of several mono-imidazole ligated complexes of (*meso*-tetramesitylporphyrinato)Fe(III) exhibiting different contributions of the $S=3/2$ state to the quantum mechanically admixed $S=5/2$, $S=3/2$ spin state. Adapted from reference [87]



provided ligand, typically histidine, is axially coordinated. Examples of these proteins are the met-myoglobin from red muscle of the shark *G. japonicus* [95] and the monomeric met-myoglobin from the buccal muscle of the sea hare *Aplysia limacina* [96]. These two coordination states of high-spin ferric hemes display very different *meso*-H resonances; the hexacoordinated myoglobins and hemoglobins display *meso*-H resonances near 40 ppm, whereas the pentacoordinated myoglobins exhibit *meso*-H resonances at approximately -20 ppm [29, 95, 96]. However, severe line broadening of these resonances can prevent the observation of *meso*-H resonances in high-spin heme proteins. A recent study with model ferrihemes has demonstrated that C_m resonances from pentacoordinated high-spin complexes occur between 500 and 700 ppm, while C_m resonances from the hexacoordinated high-spin complexes are found between 0 and 80 ppm [97]. It was therefore suggested that the C_m resonances from enzymes reconstituted with isotopically labeled heme might constitute a good tool for the straightforward determination of coordination structure in ferric high-spin heme proteins [97].

Ferrihemes possessing the $S=2$, $(d_{xy})^2(d_{xz}, d_{yz})^2(d_z^2)^1$ spin state have been shown to exhibit complicated distortions from planarity [85, 98, 99], which suggests they might exist in solution as a complex mixture of interconverting conformers with similar energies. Nonplanar hexacoordinated ferrihemes possessing a pure $S=3/2$ spin state also exhibit a unique pattern of ^{13}C NMR shifts [86] with very large downfield β shifts ($\approx 1,000$ ppm), large downfield C_α shifts (≈ 600 ppm), and large upfield C_m shifts (≈ -300 ppm) (Fig. 10d). The large downfield shifts of the C_α and C_β carbons are consistent with the presence of unpaired electron density in each of the d_{xz} and d_{yz} orbitals, which are delocalized into the $3e(\pi)$ porphyrin orbital. Since this porphyrin orbital has zero electron density at the *meso* carbons, the large upfield C_m shift stems from spin polarization from the neighboring C_α carbon. Cytochromes *c'* are a unique class of heme proteins found in photosynthetic, denitrifying and nitrogen-fixing bacteria, which exhibit unusual EPR spectra that have been ascribed to a quantum mechanical admixture of high-spin ($S=5/2$) and intermediate-spin ($S=3/2$) states [100]. The relative contribution of $S=3/2$ to the quantum mechanically admixed $S=3/2$, $S=5/2$ spin state can vary and this

has a profound effect on the ^1H [101] and ^{13}C NMR spectra [87] of ferrihemes possessing the quantum mechanical spin admixed, $S=5/2$, $S=3/2$, spin state. Thus, as the $S=3/2$ contribution increases, the C_α and C_β resonances shift upfield from approximately 1,200 ppm for a pure $S=5/2$ state to about 600 ppm (C_β) and about 400 ppm (C_α) for approximately 50% $S=3/2$ contribution. Interestingly, the C_m resonances are almost insensitive to the contribution of $S=3/2$ to the admixed $S=5/2$, $S=3/2$ spin system [87] (Fig. 11).

The pronounced differences between the ^{13}C NMR spectra of ferrihemes with $S=1/2$, d_π and $S=1/2$, $(d_{xy})^1$ electronic structure were used to study ferric hemes aimed at modeling the electronic structure of the ferric hydroperoxide ($\text{Fe}^{\text{III}}\text{-OOH}$) [102]. This oxidizing species in heme oxygenase is known to hydroxylate the heme to produce *meso*-hydroxyheme, the first stable intermediate in the pathway of heme catabolism [103]. The ^{13}C -ENDOR spectrum of $\text{Fe}(\text{III})\text{-meso-}^{13}\text{C}$ -tetraphenylporphyrin, axially coordinated by a methoxide and a *tert*-butyl-hydroperoxide ligand [$\text{meso-}^{13}\text{C-TPPFe}(\text{OCH}_3)(\text{OO}^t\text{Bu})^-$], showed that at very low temperatures (8 K) the unpaired electron resides in a d_π orbital. On the other hand, the variable-temperature ^{13}C NMR spectra of [$\text{meso-}^{13}\text{C-TPPFe}(\text{OCH}_3)(\text{OO}^t\text{Bu})^-$] suggested a situation in which a heme with a d_π electron configuration and planar porphyrinate ring is in equilibrium with a ruffled ferric porphyrinate possessing a $(d_{xy})^1$ electronic configuration. These findings led to the hypothesis that at ambient temperatures ferrihemes axially coordinated by a peroxide ligand are likely to have the $(d_{xy})^1$ electronic configuration [102]. Significant about this electronic configuration is the fact that ferric porphyrinates possessing an unpaired electron in the d_{xy} orbital are significantly ruffled and place a relatively large amount of spin and electron density at the porphyrin *meso* carbons [15, 89, 91, 104] (see Fig. 10). Therefore, these characteristic properties of $(d_{xy})^1$ ferric porphyrinates have been hypothesized to aid the attack of the terminal oxygen of the $\text{Fe}^{\text{III}}\text{-OOH}$ intermediate in heme oxygenase on the *meso* carbon [102], thus leading to the formation of *meso*-hydroxyheme [6].

In an attempt to probe the electronic structure of the hydroperoxide complex of heme oxygenase ($\text{Fe}^{\text{III}}\text{-OOH}$) at ambient temperatures, the hydroxide complex of this enzyme ($\text{Fe}^{\text{III}}\text{-OH}$) was studied by ^{13}C NMR spectroscopy. The ^{13}C NMR spectra of the $\text{Fe}^{\text{III}}\text{-OH}$ complex of heme oxygenase reconstituted with heme labeled at the core porphyrin carbons are shown in Fig. 12A and B. The resonances boxed in red correspond to a population possessing the pure $S=3/2$ spin state, as can be seen from the unique pattern of resonances in which the C_β carbons resonate near 1,000 ppm, the C_α carbons near 700 ppm, and the C_m carbons near -200 ppm. The presence of a population with the $S=1/2$, $(d_{xy})^1$ spin state is apparent from the resonances boxed in black, with the characteristic C_m resonances near 1,300 ppm and C_α resonances near -400 ppm. The most abundant population was attributed to an $S=1/2$, $S=3/2$ spin state crossover that is characterized by C_α and C_β resonances between 300 and 600 ppm and C_m resonances near zero ppm, which has been recently ob-

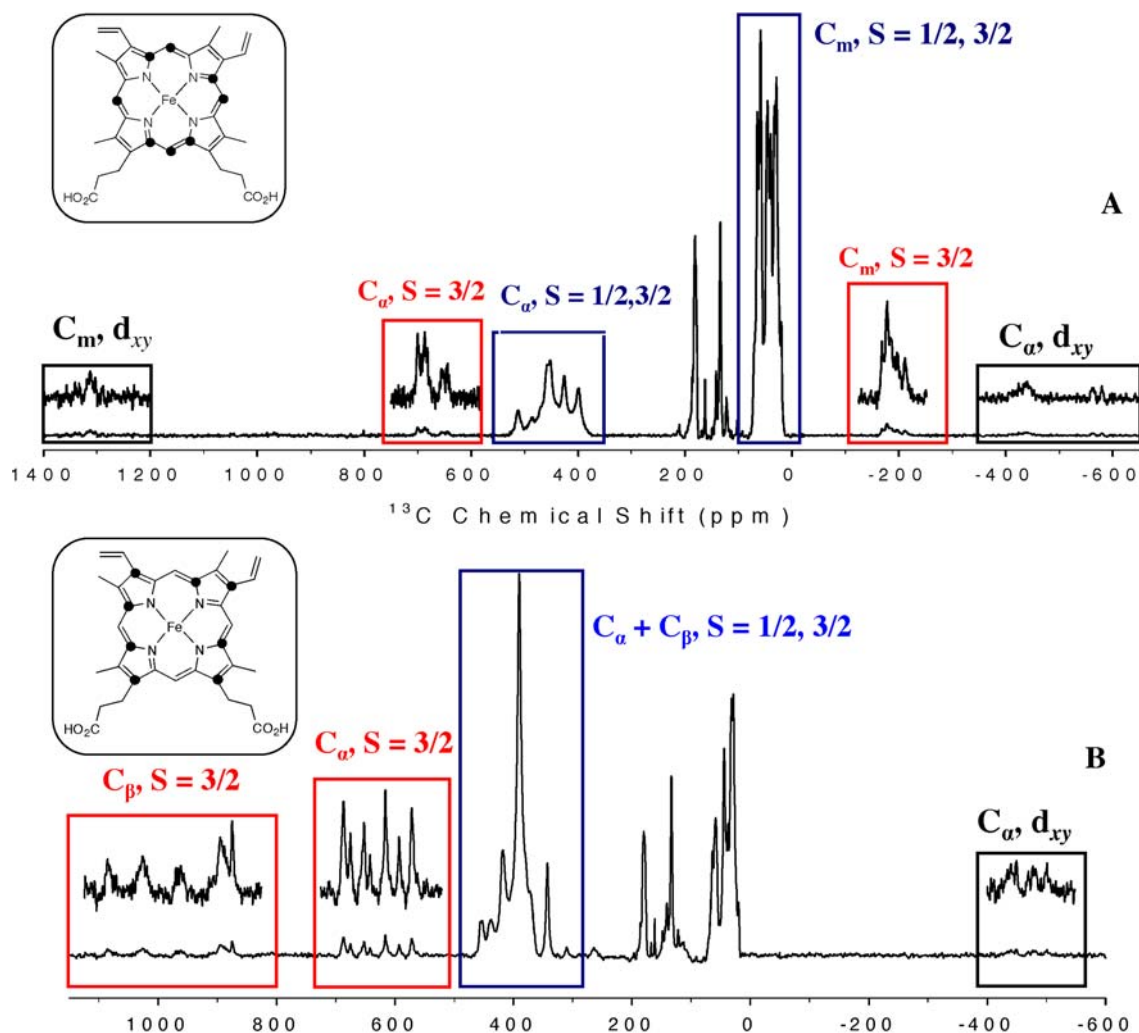


Fig. 12A,B ^{13}C NMR spectra (37°C) of the hydroxide complex of *pa*-HO (pH 10.3) reconstituted with heme labeled at the C_α and C_m (A) and C_α and C_β carbons (B). Peaks corresponding to the population exhibiting the $S=1/2$, $3/2$ spin state crossover are highlighted by blue boxes, peaks corresponding to the population with the $S=3/2$ spin state are highlighted by red boxes, and those corresponding to the population with the $S=1/2$, (d_{xy})¹ electron configuration are highlighted by black boxes. This figure was reproduced from reference [70]

served in a model ferriheme complex [85]. The presence of these unusual spin states, which are typically accompanied by large nonplanar deformations of the macrocycle, were interpreted to suggest that the water molecules in the distal pocket of HO lower the ligand field strength of the coordinated hydroxide by virtue of hydrogen bonding. The decrease in ligand field strength of the hydroxide would increase the ligand field strength of the porphyrin, thereby inducing nonplanar deformations of the porphyring ring. Hence, if the ligand field strength of the OOH^- ligand in heme oxygenase is modulated in a similar manner, the nonplanar heme and unpaired electron density at the *meso* carbons (manifested by large C_m shifts) would be expected to aid in the attack of the porphyrin by the coordinated peroxide ligand [69].

^{13}C NMR shifts, axial ligands, and axial ligand geometry

The electron configuration of the ferric iron in heme, d^5 , typically requires two strong-field ligands to stabilize the low-spin ($S=1/2$) state. Thus, ferric heme proteins exhibiting a low-spin state typically employ the histidine imidazole, the methionine thioether, or the cysteine thiolate as the axial ligands. Many of the cytochromes *c* and cytochrome *b*₅₆₂ from *E. coli* exhibit a histidine and a methionine as axial ligands [105], whereas cytochromes *b*₅, microsomal [106] or mitochondrial [71], and the four hemes of cytochrome *c*₃ [107] possess a bishistidine-coordinated heme. By comparison, the globins, including the inactive, Fe^{III} (met) forms of hemoglobin, myoglobin [4], and monomeric hemoglobins [108], as well as heme oxygenase [10, 11], the NO-carrying nitrophorins [109], and the peroxidases [29] have only one histidine axial ligand. Most of the molecules in the last group exhibit a water molecule (weak-field ligand) coordinated at the sixth position and are thus in the $S=5/2$ high-spin state. NMR spectroscopic studies of the paramagnetic active site of these high-spin proteins are typically conducted in the

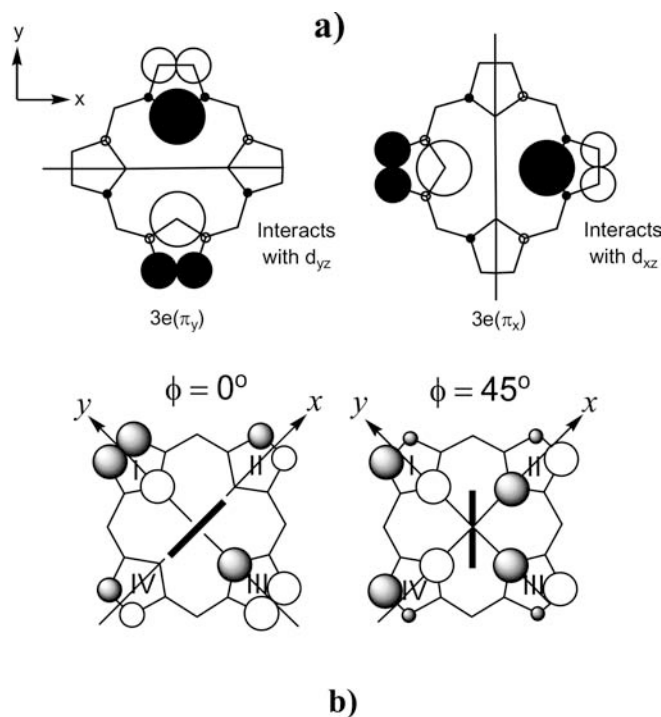


Fig. 13 a Electron density and nodal properties of porphyrin $3e(\pi)$ orbitals [110], which interact with the d_{xz} and d_{yz} orbitals of low-spin Fe(III), respectively. **b** Spin density for two angles of the proximal histidine plane (represented by a *thick black line*), $\phi=0^\circ$ and $\phi=45^\circ$, with respect to the axis along the nitrogen atoms of pyrrole rings II and IV. The size of the *circles* is proportional to the electron density at each position. Adapted from references [111] and [15]

presence of an exogenous strong-field ligand that binds (or replaces the aqua ligand) at the sixth position, therefore converting the heme protein to its low-spin state. The $S=1/2$, d_π spin state is most commonly attained and the discussion below pertains only to this electronic configuration. The exogenous strong-field ligands are typically cyanide, imidazoles, pyridines, or azide, although cyanide is sometimes preferred because its cylindrical symmetry does not introduce a perturbation of the symmetry of the porphyrin π molecular orbitals.

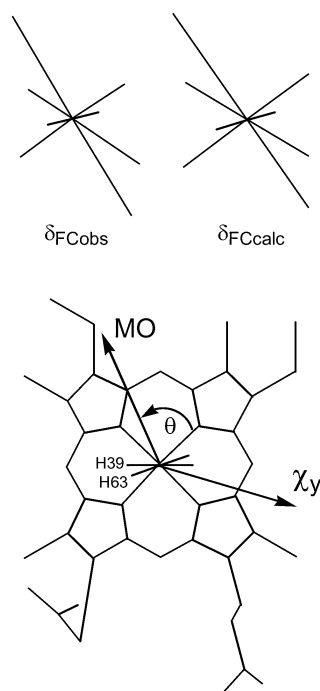
Early work conducted with met-myoglobin-cyanide revealed that the heme methyl groups exhibit significant C_2 symmetry in that the methyl group resonances appear to be grouped pairwise in that the proton NMR spectrum [110]; two methyl resonances exhibit large hyperfine shifts (≈ 20 ppm) and the other two display significantly smaller shifts, resonating at approximately 8 ppm. It is nowadays clear that the orientation of planar axial ligands exerts a large influence on the spread of the methyl resonances originating from low-spin ferric heme proteins, as well as in low-spin porphyrinates [16, 111, 112]. The fundamental property that brings about this spread in the chemical shift of heme substituents is the interaction of the proximal histidine ligand with the iron-centered e -symmetry d orbitals, which in turn, individually interact with porphyrin $3e(\pi)$ orbitals. These interactions, which have been

presented in pictorial form [15, 89, 111], can be readily understood by considering the degenerate pair of porphyrin $3e(\pi)$ molecular orbitals (Fig. 13a), which interact with the d_{xz} and d_{yz} orbitals of low-spin Fe(III). The histidine imidazole π orbitals lie perpendicular to the plane of the imidazole ring, thus these orbitals interact with the iron d_{xz} and d_{yz} orbitals and the porphyrin $3e(\pi)$ orbitals. This interaction, which can be thought of as being modulated by the angle the imidazole plane makes with the axis along the nitrogen atoms of pyrrole rings II and IV, lifts the degeneracy of the $3e(\pi)$ orbitals, alters their relative energy difference, and largely determines the degree of uneven distribution of electron spin density among the four pyrrole rings in the porphyrin macrocycle (see Fig. 13b) [111, 113]. More recently the concept of counter rotation of the g or χ tensor with rotation of axial ligand planes away from the N–Fe–N axes in the heme has been used to predict the orientation of the in-plane magnetic axis utilizing ^{13}C NMR [25, 114, 115, 116, 117, 118] and ^1H NMR [119, 120] spectroscopic data. These two approaches are summarized below.

It has been mentioned above that the contact shifts of ^{13}C nuclei bound to pyrrole β carbons, that is, the heme methyl and heme propionate α carbons, are dominated by polarization of the carbon s electrons as a consequence of unpaired electron density (p^π_{CC}) on the π orbital of the adjacent pyrrole β carbon (see Eqs. 4 and 7) [20]. Hence, an approach aimed at determining the geometry of the axial ligands has been developed based on the premise that the hyperfine shifts of ^{13}C nuclei bound to pyrrole β carbons are well suited for this purpose because these shifts are a good approximation of the corresponding contact shift [114]. This assumption is based on the fact that the dipolar contribution to the isotropic shift is small compared to the contact contribution [25], and can therefore be ignored. By comparison, in the case of ^1H nuclei, the dipolar and contact shifts are of approximately equal magnitudes [17, 25, 107, 114]; thus, δ_{dip} cannot be ignored. Since the hyperfine shift is the sum of several contributions, including the diamagnetic shift (see Eqs. 1, 2, and 3), it is possible to obtain the ^{13}C contact shift if the diamagnetic contribution is known; the value of δ_{dia} is typically obtained from the same protein in its reduced, typically low-spin $S=0$, diamagnetic form [121].

The contact shifts of ^{13}C nuclei bound to pyrrole β carbons reflect the unpaired spin distribution in the two degenerate $e(\pi)$ molecular orbitals in an idealized porphyrin with D_{4h} symmetry. If a rhombic perturbation [110] is applied, which might be thought of as changing the orientation of the axial ligand planes with respect to the heme, it mixes the orbitals and lifts the degeneracy of the $e(\pi)$ molecular orbitals. The contact shifts of the heme substituents attached to the pyrrole β carbons obtained from this model can be described by the following parameters [114]: (1) the constant Q^C_{CC} , which represents the degree of s electron polarization induced by a π electron on an adjacent carbon, (2) molecular orbital coefficients c_1 and c_5 (in the nomenclature of Longuet–Higgins [122]), which appear to show little variation among different proteins

Fig. 14 *Top* schematic representation of the observed and calculated intensities for the Fermi contact shifts, δ_{con} (observed) and δ_{con} (calculated), respectively, for the ^{13}C nuclei bound to pyrrole β carbons in the **A** isomer of bovine ferricytochrome b_5 . *Bottom* MO and χ_y represent the orientations of the rhombic perturbation of the molecular orbitals and the magnetic y axis, respectively. Note that the magnetic axis is rotated in the opposite sense to the rhombic perturbation with respect to the iron nitrogen bonds. This figure was reproduced from reference [116]



[27, 114, 116, 117, 123], (3) the orbital mixing parameter θ , and (4) the energy separation of the two $e(\pi)$ orbitals, ΔE , which is well described by a simple Boltzmann distribution between the two perturbed orbitals. Typically, a set of δ_{con} values from a heme is fitted with only three parameters, namely Q_{CC}^{C} , θ , and ΔE , while fixing the c_1 and c_5 coefficients with the most accurate values available [123]. The orientation of the rhombic perturbation (MO in Fig. 14), which is equivalent to the mixing parameter θ , is related to the orientation of the largest component of the susceptibility tensor χ_y by rotation in the opposite sense (counter rotation), relative to the axis along the nitrogen atoms of pyrrole rings II and IV [116, 123]. The orientation of the rhombic perturbation (MO) has been shown to correlate well with the average of the normals to the imidazole planes of several bishistidine-ligated ferricytochromes c_3 [107, 114, 117], cytochrome c'' [56] and cytochrome c_6 [27], thus allowing the determination of their axial ligand geometries.

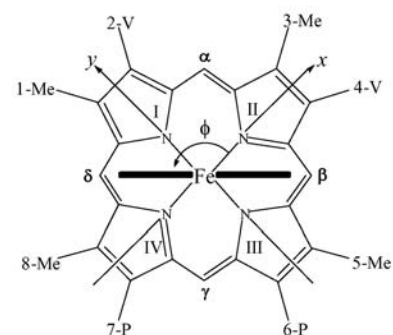
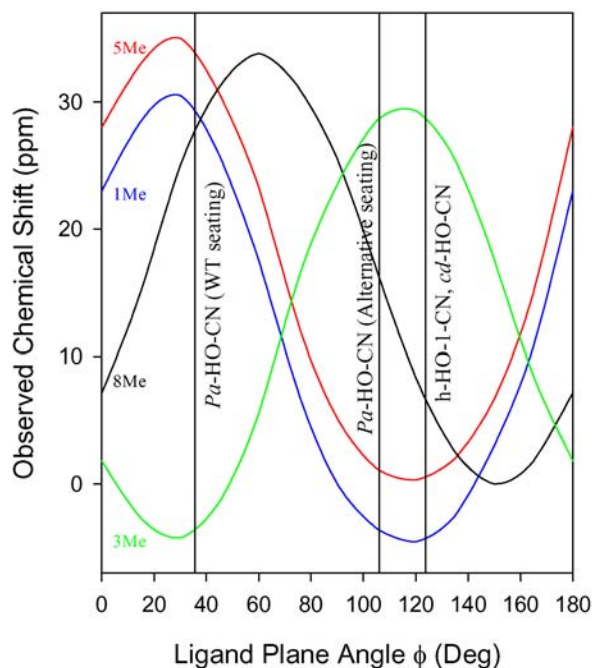
This analysis of ^{13}C NMR data, which was developed using data sets from cytochrome c , has been extended to b hemes, such as those found in cytochrome b_5 [115, 116], myoglobin [115], and the peroxidases [123]. In the b hemes the vinyl carbons experience shifts caused by delocalization of unpaired electron density from the heme π molecular orbitals, in addition to the aforementioned polarization of the carbon s electrons by unpaired electron density in the π orbital of the neighboring pyrrole β carbon. The δ_{con} corresponding to the vinyl groups was corrected by a constant derived from theoretical treatment [115] and from an empirical correction factor [116, 123]. Results obtained with cytochrome b_5 were in reasonable agreement with the average of the orientations of the normals to the His-imidazoles observed in the crystal struc-

ture [106] of this protein. This was interpreted as an indication that the two His ligands in cytochrome b_5 have approximately equal influence on the electronic structure and that together they dominate the rhombic perturbation. This result is in contrast to previous conclusions derived from a ^1H NMR spectroscopic study which suggested that one of the His ligands (His-39) dominates the magnetic properties of cytochrome b_5 [124]. It has been pointed out that the origin of the significant differences in the ^1H shifts originating from the $\beta\text{-CH}_2$ groups of His-39 and His-63, which were interpreted as evidence of the dominant influence of His-39 [125], might originate from conformational differences [116]. Support for this hypothesis has been postulated [116] to come from the fact that the ^{13}C shifts of the $\beta\text{-CH}_2$ groups in His-39 and His-63 can be seen close to each other (ca. 20 ppm) in the HMQC spectrum of Fig. 2 reported by Lee et al. [126].

The effect of axial ligand nodal plane orientation on the contact and dipolar ^1H shifts of low-spin ferrihemes has been calculated as a function of the angle of the axial ligand plane with respect to the axis along the nitrogen atoms on pyrrole rings II and IV [119]. Estimates of the δ_{con} contribution to the isotropic shift were obtained from Hückel methods. Calculations of g anisotropy assuming counter rotation of the g tensor [120] were used to estimate the contribution of δ_{dip} . It was found that for systems having one axial ligand, or two axial ligands in parallel planes, the δ_{con} and δ_{dip} contributions to the isotropic shift are comparable at the *meso*-hydrogen position, whereas the contact contribution dominates the isotropic shifts of heme methyl groups. The predicted isotropic shifts were plotted as a function of axial ligand nodal plane orientation for b - and c -type hemes (Fig. 15) [119]. These plots, which represent a straightforward visual aid to estimate the orientation of the axial ligands, show very good agreement in the order of the predicted shifts, and reasonable agreement in the magnitude of the shifts. This approach has been made more quantitative with the finding of equations that describe the relationship between axial ligand geometry and ^1H shifts [127, 128] for c and b hemes and ^{13}C [128] shifts for c hemes.

The plot shown in Fig. 15 summarizes calculations in the case of b hemes axially coordinated by proximal histidine and distal cyanide ligands, or by two histidine ligands parallel to one another [119]. The plot permits the straightforward correlation of the observed shifts for the four heme methyl groups (1Me, 3Me, 5Me, and 8Me) as a function of the angle ϕ formed between the axial ligand plane and the molecular x axis. By using the information in this plot and the NMR resonance assignments obtained for the heme methyl groups [58, 129], it was possible to correctly predict an angle ϕ of 125° for the proximal imidazole plane of human heme oxygenase [119] before the X-ray crystal structure was obtained [10]. Thus, the calculations summarized in the plot of Fig. 15 provide a straightforward predictive framework to study heme-containing proteins and enzymes even if their structure is not available. More recently a study has been published that correlates the order of heme methyl resonances in the

Fig. 15 Right right-handed coordinate system and nomenclature used for describing the projection of the His-imidazole plane onto the porphyrin ring. The x axis is aligned along the nitrogen atoms of pyrrole rings II and IV of the heme, the y axis is along the nitrogen atoms of pyrrole rings I and III, and the z axis is normal to the heme. *Left* dependence of observed heme methyl shifts on the angle ϕ formed between the molecular x axis and the projection of the imidazole plane. Adapted from reference [119]



high-spin form of several ferriheme proteins [94]. There is an apparent 90° shift in the nodal plane of the orbital involved in spin delocalization compared to the histidine-imidazole plane. This 90° rotation has been explained in terms of almost complete use of only one of the d_π (d_{xz} or d_{yz}) metal orbitals to delocalize electron density into one of the two $4e(\pi^*)$ porphyrin orbitals [94].

From the discussion above it is apparent that the predictive power of the calculations summarized in the plot of Fig. 15 depends on unambiguous assignments of the four heme methyl resonances. In certain cases enzymes reconstituted with ^{13}C -labeled hemes can be used to facilitate the assignment process or to obtain unambiguous assignments of methyl resonances buried under the envelope of polypeptide signals. This approach was applied to the study of heme oxygenase from *Pseudomonas aeruginosa* (*pa*-HO). This bacterial heme oxygenase is unique in that it oxidatively cleaves the heme at the δ -*meso* carbon [130], whereas all other known heme oxygenases, mammalian and bacterial, cleave the heme exclusively at the α -*meso* carbon (see [7] and references therein). The magnitude and spread of the assigned heme methyl resonances from *pa*-HO, interpreted in the context of the plot shown in Fig. 15, indicated that the histidine imidazole plane in this enzyme forms an angle ϕ of approximately 35° with respect to the molecular x axis [69] (see Fig. 15). This finding strongly suggested that the heme in *pa*-HO is seated within the polypeptide in a manner that is distinct from that observed for all other heme oxygenases for which a structure is known. Furthermore, it was concluded that the unique oxidative regioselectivity of *pa*-HO is a consequence of the heme being rotated in-plane by approximately 100° relative to the orientation (seating) of the heme in all α -oxidizing heme oxygenase enzymes of known structure because the in-plane rotation places the

δ -*meso* carbon within the heme oxygenase fold in the place where the α -oxidizing enzymes typically place the α -*meso* carbon [69].

The Asn19Lys/Phe117Tyr double mutant of *pa*-HO was constructed to probe the hypothesis that the unusual heme seating in *pa*-HO is brought about by the absence of hydrogen bonding and electrostatic contacts between the heme propionates and residues at position 19 and 117 [69]. Thus, introducing Lys-19 and Tyr-117 was expected to restore these interactions, which are present in all α -oxidizing heme oxygenases of known structure [10, 11]. The high-frequency portion of the ^1H NMR spectrum of the double mutant (Fig. 16) displays a large number of resonances; the resonances labeled with arrows and asterisks, as well as those highlighted by dotted arrows and circles were unequivocally shown to originate from heme methyl groups. This information was obtained from the HMQC spectrum of Fig. 16, which was acquired from a sample of mutant enzyme reconstituted with heme labeled as in Fig. 5A. The presence of 15 cross peaks strongly suggested that the Asn19Lys/Phe117Tyr double mutant of *pa*-HO exists in solution as a mixture of four different molecules: two different heme seatings create a set of two and heme orientational isomerism creates a subset of two from each heme seating isoform [69]. Exchange spectroscopy (EXSY) was used to demonstrate that the heme methyl peaks labeled by arrows, which correspond to enzyme exhibiting the heme seating characteristic of the wild type enzyme, are in dynamic exchange with a new heme seating, which exhibits the heme methyl resonances labeled by asterisks. The chemical shifts of the heme methyl groups interpreted in the context of the plot in Fig. 15 were used to conclude that the heme in the mutant enzyme displays a dynamic equilibrium between two heme seatings (shown in Fig. 17) that differ by an in-plane rotation of approximately

Fig. 16 HMQC spectrum of the cyanide-inhibited Asn-19 Lys/Phe-117 Tyr double mutant of heme oxygenase from *Pseudomonas aeruginosa* (*pa*-HO) reconstituted with heme derived from [1,2- ^{13}C]-ALA. Only the low-frequency (^{13}C) region of the spectrum, which displays the heme methyl resonances, is shown. The 1-D ^1H and non-decoupled ^{13}C spectra are shown to illustrate the J_{CH} splittings. Arrows and dashed arrows, respectively, represent the major and minor orientational isomers exhibiting the wild type heme seating. Asterisks and open circles, respectively, represent the major and minor orientational isomers exhibiting the alternative seating. This figure was reproduced from reference [69]

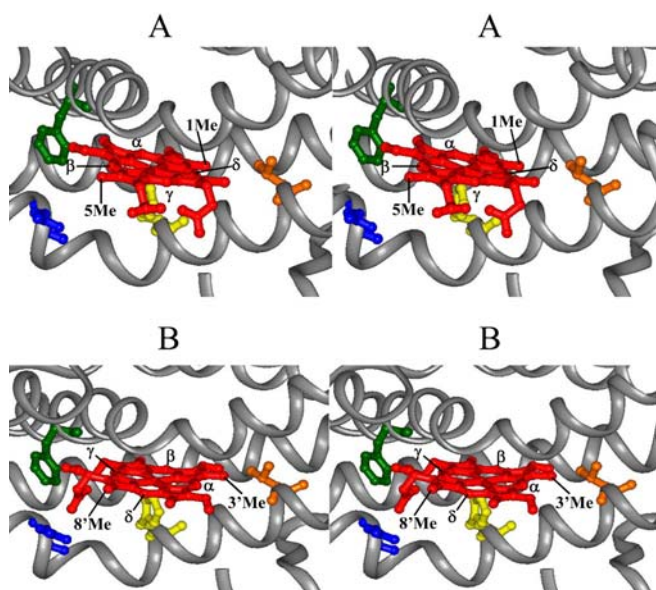
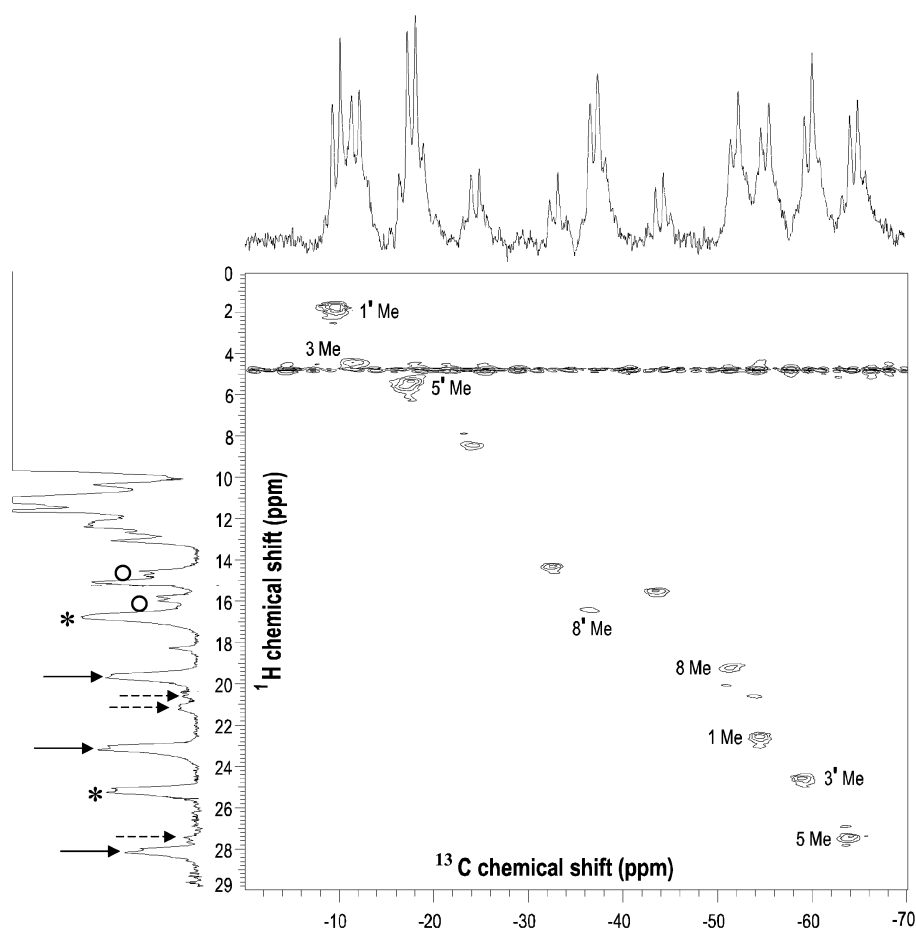


Fig. 17A,B Stereoview of the predicted wild type (A) and alternative (B) heme seatings in mutant *pa*-HO-CN, modeled into the fold of heme oxygenase. The heme is shown in red, Asn-19 in blue, and Phe-117 in green. The wild type seating of *pa*-HO (A) places the δ -*meso* carbon where it is susceptible to hydroxylation, whereas 110° in-plane rotation of the heme results in the alternative seating (B), thus positioning the α -*meso* carbon where it can be hydroxylated. This figure was reproduced from reference [69]

100° [69]. The unambiguous assignments of the ^1H resonances from the heme methyl groups, especially those resonating under the crowded diamagnetic region (see Fig. 16) in this complicated mixture of isoforms, was made possible by the utilization of ^{13}C -labeled heme.

In the discussion above it has been assumed that the orientation of the axial ligand dominates the asymmetry of electron spin delocalization. Other factors such as the nature of heme substituents (i.e., vinyl, methyl, and propionate), van der Waals interactions between the heme and side chains lining the heme pocket, and heme conformational distortions from planarity can provide secondary modifications of the in-plane asymmetry. A recent study pointed out that ^{13}C NMR spectroscopy is well suited to elucidate the nature and extent of these secondary regulatory mechanisms [131]. These authors demonstrated that even if the magnetic axes and anisotropies are known, the intrinsic uncertainties in the orientational parameters lead to a relatively large uncertainty in the determination of the dipolar contribution to the methyl proton isotropic shifts. By comparison, the relatively small contribution of the methyl carbon dipolar shift to the isotropic shift makes the methyl carbon contact shifts more reliable indicators of the unpaired electron distribution on the heme macrocycle [114, 131]. Thus, by utilizing the $^{13}\text{CH}_3$ pattern of non-inversion symmetry in centro- and pseudocentro-symmetric hemes reconstituted into myoglobin, it was shown that π -

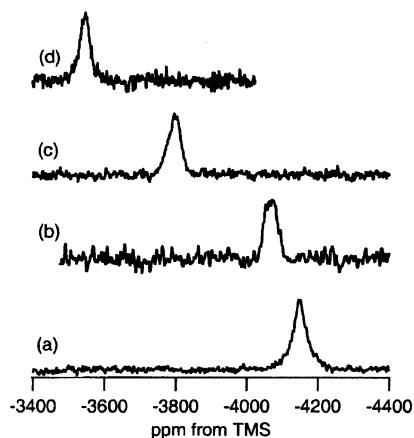


Fig. 18a–d ^{13}C NMR spectra of ferric heme proteins coordinated by ^{13}CN . **a** Sperm whale myoglobin in 0.1 M phosphate buffer, pH=7.0. **b** Human hemoglobin in 0.1 M Tris-HCl buffer, pH=7.0. **c** Horse heart cytochrome *c* in 0.1 M phosphate buffer, pH=7.0. **d** Horseradish peroxidase in 0.1 M phosphate buffer, pH=7.0. This figure was reproduced from reference [135]

π interactions between the heme and aromatic residues in close contact perturb the in-plane asymmetry of unpaired electron distribution. Hence, it is likely that in the quantitative interpretation of heme methyl ^{13}C contact shifts in the context of axial ligand plane orientation in *b* hemes, the regulatory effect of π - π interactions will have to be taken into account [131]. Furthermore, it is important to investigate whether these secondary modulations of in-plane asymmetry have important functional consequences.

A number of studies have been reported that utilize ^{13}C -enriched carbon monoxide (CO) bound to the distal site of ferrous heme proteins. These studies have typically been aimed at understanding the nature of the distal pocket in globins and other heme proteins [46, 47, 132, 133]. Recently, the ^{57}Fe chemical shift has been found to correlate well with the C_m chemical shift of CO complexes of several Fe(II) metalloporphyrins. Consequently, the hard-to-observe ^{57}Fe chemical shifts can be predicted from the C_m chemical shifts in carbonmonoxy complexes of Fe(II) [133]. The C_m shifts from these carbonmonoxy complexes have also been shown to correlate with the average displacement of the *meso* carbon atoms from the plane (ruffling) of the macrocycle.

^{13}C and ^{15}N NMR spectroscopy have also been used to study the environment and electronic structure of low-spin ferriheme centers by observing the ^{13}C [134, 135] and the C^{15}N resonance [136, 137] of bound cyanide. The ^{15}N resonance was found to be extremely sensitive to the polarity of the distal pocket and the nature of the proximal ligand, with the consequence that it is very difficult to factor out the two effects. A recent report demonstrated convincingly that the ^{13}C resonance from biscyano protoheme IX occurs far upfield, $-2,516$ ppm. By comparison, the ^{13}C resonance from the cyanide-imidazole complex of protoheme IX was found much further upfield, $-3,926$ ppm, and that corresponding to the cyanide-imidazolate

complex was found at $-3,507$ ppm. These findings indicate that the nature of the proximal ligand in heme proteins can be elucidated from the chemical shift of the ^{13}C resonance [135]. In fact, the ferric cyanide complexes of myoglobin, hemoglobin, cytochrome *c*, and horse radish peroxidase exhibit their corresponding ^{13}C resonance at $-4,154$, $-4,074$, $-3,761$, and $-3,543$ ppm, respectively (Fig. 18). The values of these resonances correlate well with the imidazolate character of the proximal histidine, which increases in the order of myoglobin, hemoglobin, cytochrome *c*, and horseradish peroxidase [135].

Concluding remarks and outlook

It is apparent that the analysis of heme proteins and model heme complexes by ^{13}C NMR spectroscopy can provide important information regarding the electronic and coordination state of paramagnetic heme proteins and model hemes. The initial lag in the application of ^{13}C NMR spectroscopy to the analysis of paramagnetic heme proteins is no doubt a consequence of low sensitivity and low natural abundance. However, revolutionary developments in methodology and instrumentation in the field of NMR spectroscopy, together with the advent of recombinant DNA methods that permit the relatively simple expression and purification of adequate amounts of protein, have largely contributed to the successful application of ^{13}C NMR spectroscopy to the study of paramagnetic heme proteins. The more recent development of highly sensitive probes with superconducting frequency coils cooled below their critical temperature (CryoProbes) and the availability of ^{13}C -labeled hemes is expected to further attenuate the limitations imposed by the low sensitivity and low natural abundance of ^{13}C nuclei, so that the observation of core porphyrin carbons in paramagnetic heme proteins may become as commonplace as the current observation of protonated heme carbons. Furthermore, the utilization of CryoProbes allows one to increase the sensitivity of the experiment without necessarily increasing the applied magnetic field. This is likely to have important repercussions in the analysis of paramagnetic shifts of relatively large heme proteins because the Curie spin relaxation effect on T_2^{-1} , which affects line broadening, varies as the square of the applied magnetic field [35]. Finally, it is also noteworthy that enhanced paramagnetic relaxation can result in non-detectable NOE correlations that involve protons on histidine-imidazoles that are coordinated to the ferric heme iron, thus leaving the structure of the heme active site ill defined in protein structures. Thus, the analysis of ^{13}C contact shifts aimed at obtaining the geometry of axial ligands is likely to render important complementary information that permits an improvement in the structure of the heme active site in the structures of paramagnetic heme proteins in solution [27, 138].

Acknowledgments The authors' research reported in this manuscript was carried out with support from grants from the National Institutes of Health (GM 50503) and the National Science Foundation (MCB-0110139).

References

1. Turano P, Lu Y (eds) (2001) Iron in heme and related proteins. In: Bertini I, Sigel A, Sigel H (eds) *Handbook on metalloproteins*, vol 9. Marcel Dekker, New York, pp 269–356
2. Scott RA, Mauk AG (eds) (1996) *Cytochrome c. A multidisciplinary approach*. University Science Books, Sausalito, CA
3. Sono M, Roach MP, Coulter ED, Dawson JH (1996) *Chem Rev* 96:2841–2847
4. Springer BA, Sligar SG, Olson JS, Phillips GN Jr (1994) *Chem Rev* 94:699–714
5. Agron PG, Ditta GS, Helinski DR (1993) *Proc Natl Acad Sci USA* 90:3506
6. Ortiz de Montellano PR (2000) *Curr Opin Chem Biol* 4:221–227
7. Ortiz de Montellano PR, Wilks A (2000) *Adv Inorg Chem* 51:359–407
8. Ribeiro JMC, Hazzard JM, Nussenzweig RH, Champagne DE, Walker FA (1993) *Science* 260:543
9. Bellamy TC, Garthwaite J (2002) *Mol Cell Biochem* 230:165–176
10. Schuller DJ, Wilks A, Ortiz de Montellano PR, Poulos TL (1999) *Nature Struct Biol* 6:860–867
11. Schuller DJ, Zhu W, Stojiljkovic I, Wilks A, Poulos TL (2001) *Biochemistry* 40:11552–11558
12. La Mar GN, de Ropp JS (1993) NMR methodology for paramagnetic proteins. In: Berliner LJ, Reuben J (eds) *Biological magnetic resonance*. Plenum, New York, pp 1–111
13. Satterlee JD (1990) *Concepts Magn Reson* 2:69–79
14. Kurland RJ, McGarvey BR (1970) *J Magn Reson* 2:286
15. Walker FA (2000) Proton NMR and EPR spectroscopy of paramagnetic metalloporphyrins. In: Kadish KM, Smith KM, Guillard R (eds) *The porphyrin handbook*. Academic Press, San Diego, pp 81–183
16. Satterlee JD (1986) *Annu Rep Nucl Magn Reson Spectrosc* 17:79–178
17. Bertini I, Luchinat C (1996) *Coord Chem Rev* 150:1–296
18. Wüthrich K, Baumann R (1973) *Helv Chim Acta* 56:585–596
19. McConnell HM (1956) *J Chem Phys* 24:764–766
20. Karplus M, Fraenkel GK (1961) *J Chem Phys* 35:1312–1323
21. Wüthrich K, Baumann R (1974) *Helv Chim Acta* 57:336–350
22. Wüthrich K, Billeter M, Braun W (1983) *J Mol Biol* 180:715–740
23. Mispelter J, Momenteau M, Lhoste JM (1993) Heteronuclear magnetic resonance applications to biological and related paramagnetic models. In: Berliner LJ, Reuben J (eds) *Biological magnetic resonance*. Plenum, New York, pp 299–355
24. Goff HM (1981) *J Am Chem Soc* 103:3714–3722
25. Turner DL (1993) *Eur J Biochem* 211:563–568
26. Banci L, Bertini I, Pierattelli R, Vila JA (1994) *Inorg Chem* 33:4338–4343
27. Louro RO, Medina M, Aguiar AP, Hervas M, De la Rosa M, Gomez-Moreno C, Turner DL, Xavier AV (1998) *J Biol Inorg Chem* 3:68–73
28. Bertini I, Turano P (1995) The hyperfine coupling. In: La Mar GN (ed) *Nuclear magnetic resonance of paramagnetic molecules*. Kluwer, London, pp 29–54
29. La Mar GN, Satterlee JD, De Ropp JS (eds) (2000) Nuclear magnetic resonance of hemoproteins. In: Kadish KM, Smith KM, Guillard R (eds) *The porphyrin handbook*, vol 5. Academic Press, pp 185–297
30. Gueron M (1975) *J Magn Reson* 19:58–66
31. Vega AJ, Fiat D (1976) *Mol Phys* 31:347–355
32. Unger SW, Jue T, La Mar GN (1985) *J Magn Reson* 61:448–456
33. Solomon I (1955) *Phys Rev* 99:559–565
34. Bloembergen (1957) *J Chem Phys* 27:572–573
35. Satterlee JD (1990) *Concepts Magn Res* 2:119–129
36. Banci L (1993) Nuclear relaxation in paramagnetic proteins. In: Berliner LJ, Reuben J (eds) *Biological magnetic resonance*. Plenum, New York, pp 79–112
37. Yamamoto Y (1994) *J Magn Reson* B103:72–76
38. La Mar GN, de Rop JS (1993) NMR methodology for paramagnetic proteins. In: Berliner LJ, Reuben J (eds) *Biological magnetic resonance*. Plenum, New York, pp 1–78
39. Sankar SS, LaMar GN, Smith KM, Fujinari EM (1987) *Biochim Biophys Acta* 912:220–229
40. Satterlee JD, Alam S, Yi Q, Erman JE, Constantinidis I, Russell DJ, Moench SJ (1993) Proton NMR studies of selected paramagnetic heme proteins. In: Berliner LJ, Reuben J (eds) *Biological magnetic resonance*. Plenum, New York, pp 275–297
41. Walker FA, Simonis U (1993) Proton NMR spectroscopy of model hemes. In: Berliner LJ, Reuben J (eds) *Biological magnetic resonance*, vol 12. Plenum, New York, pp 133–274
42. Banci L, Piccioli M, Scozzafava A (1992) *Coord Chem Rev* 120:1–28
43. Bertini I, Luchinat C (1999) *Curr Opin Chem Biol* 3:145–151
44. Bertini I, Luchinat C, Tarchi D (1993) *Chem Phys Lett* 203:445–449
45. Bertini I, Luchinat C, Piccioli M, Tarchi D (1994) *Concepts Magn Reson* 6:307–335
46. Behere DV, Gonzalez-Vergara E, Goff HM (1985) *Biochim Biophys Acta* 131:607–613
47. Moon RB, Dill K, Richards JH (1977) *Biochemistry* 16:221–228
48. Nelson MJ, Huestis WH (1980) *Biochim Biophys Acta* 623:467–470
49. Santos H, Turner DL (1985) *FEBS Lett* 184:240–244
50. Yamamoto Y (1987) *FEBS Lett* 222:115–119
51. Summers MF, Marzilli LG, Bax A (1986) *J Am Chem Soc* 108:4285–4294
52. Timkovich R (1991) *Inorg Chem* 30:37–42
53. Sukits SF, Satterlee JD (1996) *Biophys J* 71:2848–2856
54. Wei X, Ming L-J, Cannons AC, Solomonson LP (1998) *Biochim Biophys Acta* 1382:129–136
55. Santos H, Turner DL (1986) *FEBS Lett* 194:73–77
56. Costa HS, Santos H, Turner DL (1996) *Eur Biophys J* 25:19–24
57. Louro RO, Waal EC, Ubbink M, Turner DL (2002) *FEBS Lett* 510:185–188
58. Hernandez G, Wilks A, Paolesse R, Smith KM, Ortiz de Montellano PR, La Mar GN (1994) *Biochemistry* 33:6631–6641
59. Rivera M, Walker FA (1995) *Anal Biochem* 230:295–302
60. Warren MJ, Scott AI (1990) *TIBS* 15:426
61. Scott AI (1993) *Angewandte Chemie* 32:1223–1376
62. Biel SW, Biel AJ (1990) *J Bacteriol* 172:1321–1326
63. Harris WF III, Burkhalter RS, Lin W, Timkovich R (1993) *Bioorg Chem* 21:209–220
64. Rivera M, Barillas-Mury C, Christensen KA, Little JW, Wells MA, Walker FA (1992) *Biochemistry* 31:12233–12240
65. Studier FW, Moffatt BA (1986) *J Mol Biol* 189:113–130
66. Silchenko S, Sippel ML, Kuchment O, Benson DR, Mauk AG, Altuve A, Rivera M (2000) *Biochem Biophys Res Commun* 273:467–472
67. Altuve A, Silchenko S, Lee KH, Kuczera K, Terzyan S, Zhang X, Benson DR, Rivera M (2001) *Biochemistry* 40:9469–9483
68. Cowley AB, Altuve A, Kuchment O, Terzyan S, Zhang X, Rivera M, Benson DR (2002) *Biochemistry* 41:11566–11581
69. Caignan GA, Deshmukh R, Wilks A, Zeng Y, Huang H, Moënné-Loccoz P, Bunce RA, Eastman MA, Rivera M (2002) *J Am Chem Soc* 124:14879–14892
70. Caignan GA, Deshmukh R, Zeng Y, Wilks A, Bunce RA, Rivera M (2003) *J Am Chem Soc* 125:000–000
71. Rodriguez-Maranon MJ, Feng Q, Stark RE, White SP, Zhang X, Foundling SI, Rodriguez V, Schilling CL III, Bunce RA, Rivera M (1996) *Biochemistry* 35:16378–16390
72. Rivera M, Qiu F, Bunce RA, Stark RE (1999) *JBIC* 4:87–98
73. Rivera M, Seetharaman R, Ghirdhar D, Wirtz M, Zhang X, Wang X, White S (1998) *Biochemistry* 37:1485–1494
74. Rodriguez JC, Rivera M (1998) *Biochemistry* 37:13082–13090

75. Bunce RA, Shilling CL III, Rivera M (1997) *J Labelled Compd Radiopharm* 39:669–675
76. Kurumaya K, Okazaki T, Seido N, Akasaka Y, Kawajiri Y, Kajiwara M, Kondo M (1989) *J Labelled Compd Radiopharm* 27:217
77. Behr J, Hellwig P, Mäntele W, Michel H (1998) *Biochemistry* 37:7400–7406
78. Page DM, Ferguson SJ (1994) *J Bacteriol* 176:5919–5928
79. Pervushin K, Riek R, Wider G, Wüthrich K (1997) *Proc Natl Acad Sci USA* 94:12366–12371
80. Bax A, Freeman R, Frenkiel TA (1981) *J Am Chem Soc* 103:2102–2104
81. Qiu F, Rivera M, Stark RE (1998) *J Magn Reson* 130:76–81
82. Morris GA, Freeman R (1979) *J Am Chem Soc* 101:760–762
83. Mispelster J, Momenteau M, Lhoste JM (1979) *Chem Comm* 808–810
84. Ikeue T, Ohgo Y, Takashi S, Nakamura M, Fujii H, Yokoyama M (2000) *J Am Chem Soc* 122:4068–4076
85. Ikeue T, Ohgo Y, Yamaguchi M, Takahashi M, Takeda M, Nakamura M (2001) *Angew Chem Int Ed* 40:2617–2620
86. Ikeue T, Ohgo Y, Saitoh T, Yamaguchi T, Nakamura M (2001) *Inorg Chem* 40:3423–3434
87. Ikezaki A, Nakamura M (2002) *Inorg Chem* 41:6225–6236
88. Mao J, Zhang Y, Oldfield E (2002) *J Am Chem Soc* 124:13911–13920
89. Walker FA (1999) *Coord Chem Rev* 185–186:471–534
90. Walker FA, Nasri H, Torowska-Tyrk I, Mohanrao K, Watson CT, Shkhirev NV, Debrunner PG, Scheidt WR (1996) *J Am Chem Soc* 118:12109–12118
91. Safo MK, Walker FA, Raitsimring AM, Walters WP, Dolata DP, Debrunner PG, Scheidt WR (1994) *J Am Chem Soc* 116:7760–7770
92. Goff HM, Shimomura ET, Phillippi MA (1983) *J Am Chem Soc* 105:66–71
93. Phillippi MA, Goff HM (1980) *J Chem Soc Chem Commun* 455–456
94. Shokhireva TK, Shokhirev NV, Walker FA (2003) *Biochemistry* 42:679–693
95. Yamamoto Y, Osawa A, Inoue Y, Chûjô R, Suzuki T (1990) *Eur J Biochem* 192:225–229
96. Pande U, La Mar GN, Lecomte JTT, Ascoli F, Bruonori M, Smith KM, Pandey RK, Parish DW, Thanabal V (1986) *Biochemistry* 25:5638–5646
97. Nakamura M, Hoshino A, Ikezaki A, Ikeue T (2003) *Chem Comm* 1862–1863
98. Ikeue T, Saitoh T, Yamaguchi T, Ohgo Y, Nakamura M, Takahashi M, Takeda M (2000) *Chem Comm* 1989–1990
99. Simonato JP, Pécaut J, Le Pape L, Oddou JL, Jeandey C, Shang M, Scheidt R, Wojaczynski J, Wolowicz S, Latos-Grazynky L, Marchon JC (2000) *Inorg Chem* 39:3978–3987
100. Maltempo MM (1976) *Quart Rev Biophys* 9:181–215
101. Cheng R-J, Chen P-Y, Gau P-R, Chen C-C, Peng S-M (1997) *J Am Chem Soc* 119:2563–2569
102. Rivera M, Caignan GA, Astashkin AV, Raitsimring AM, Shokhireva TK, Walker FA (2002) *J Am Chem Soc* 124:6077–6089
103. Ortiz de Montellano PR (1998) *Acc Chem Res* 31:543–549
104. Simonneaux G, Schünemann V, Morice C, Carel L, Toupet L, Winkler H, Trautwein AX, Walker FA (2000) *J Am Chem Soc* 122:4366–4377
105. Mathews FS, Bethge PH, Czerwinski W (1979) *J Biol Chem* 254:1699–1706
106. Durley RCE, Mathews FS (1996) *Acta Cryst D52*:65–76
107. Turner DL, Costa HS, Coutinho IB, LeGall J, Xavier AV (1997) *Eur J Biochem* 243:474–481
108. Volkman BF, Alam SL, Satterlee JD, Markley JL (1998) *Biochemistry* 37:10906–10919
109. Weichsel A, Andersen JF, Champagne DE, Walker FA, Montfort WR (1998) *Nat Struct Biol* 5:304–309
110. Shulman RG, Glarum SH (1971) *J Mol Biol* 57:93–115
111. Walker FA (1980) *J Am Chem Soc* 102:3254–3256
112. Goff H (1980) *J Am Chem Soc* 102:3252–3254
113. Walker FA, Buehler J, West JT, Hinds JL (1983) *J Am Chem Soc* 105:6923–6929
114. Turner DL, Salgueiro CA, Schenkels P, LeGall J, Xavier AV (1995) *Biochim Biophys Acta* 1246:24–28
115. Banci L, Pierattelli R, Turner DL (1995) *Eur J Biochem* 232:522–527
116. Pierattelli R, Turner DL (1996) *Eur Biophys J* 24:342–347
117. Louro RO, Correia IJ, Brennan L, Coutinho IB, Xavier AV, Turner DL (1998) *J Am Chem Soc* 120:13240–13247
118. Yamamoto Y, Nanai N, Chûjô R, Suzuki T (1990) *FEBS Lett* 264:113–116
119. Shokhirev NV, Walker FA (1998) *J Biol Inorg Chem* 581–594
120. Shokhirev NV, Walker FA (1998) *J Am Chem Soc* 120:981–990
121. Santos H, Turner DL (1992) *Eur J Biochem* 206:721–728
122. Longuet-Higgins HC, Rector CW, Platt JR (1950) *J Chem Phys* 18:1174–1181
123. Pierattelli R, Banci L, Turner DL (1996) *J Biol Inorg Chem* 1:320–329
124. Lee K-B, La Mar GN, Mansfield KE, Smith KM, Pochaspky TC, Sligar SG (1993) *Biochim Biophys Acta* 1202:189–199
125. Lee K-B, McLachlan SJ, La Mar GN (1994) *Biochim Biophys Acta* 1208:22–30
126. Lee K-B, Kweon J, Park H (1995) *FEBS Lett* 367:77–80
127. Bertini I, Luchinat C, Parigi G, Walker FA (1999) *J Biol Inorg Chem* 4:515–519
128. Turner DL (2000) *J Biol Inorg Chem* 5:328–332
129. Gorst CM, Wilks A, Yeh DC, Ortiz de Montellano PR, La Mar GN (1998) *J Am Chem Soc* 120:8875–8884
130. Ratliff M, Zhu W, Deshmukh R, Wilks A, Stojilkovic I (2001) *J Bacteriol* 183:6394–6403
131. Hu B, Hauksson B, Tran A-TT, Kolczak U, Pandey RK, Rezzano IN, Smith KM, La Mar GN (2001) *J Am Chem Soc* 123:10063–10070
132. Kalodimos CG, Gerothanassis IP, Pierattelli R, Ancian B (1999) *Inorg Chem* 38:4283–4293
133. Kalodimos CG, Gerothanassis IP, Pierattelli R, Troganis A (2000) *J Inorg Biochem* 79:371–380
134. Goff HM (1977) *J Am Chem Soc* 99:7723–7725
135. Fujii H (2002) *J Am Chem Soc* 124:5936–5937
136. Morishima I, Inubushi T, Neya S, Ogawa S, Yonezawa T (1977) *Biochem Biophys Res Commun* 78:739–746
137. Morishima I, Inubushi T (1978) *J Am Chem Soc* 100:3568–3564
138. Turner DL, Brennan L, Chamberlin SG, Louro RO, Xavier AV (1998) *Eur Biophys J* 27:367–375
139. Yamamoto Y, Chûjô R (1992) *Chem Comm* 87–89